NASA TECHNICAL NOTE

NASA TN D-8074

NASA TN D-8074

COMPARISON OF VIBRATIONS OF A COMBINATION OF SOLID-ROCKET LAUNCH VEHICLE AND PAYLOAD DURING A GROUND FIRING AND LAUNCHING

James A. Schoenster and Harold B. Pierce

Langley Research Center
Hampton, Va. 23665

NATIONAL AERONAUTICS AND SPACE ADMINISTRATION • WASHINGTON, D. C. • DECEMBER 1975

1 Report No	2 Government Accession No	3 Recipient's Catalog No
NASA TN D-8074		

4 Title and Subtitle	5 Report Date
COMPARISON OF VIBRATIONS OF A COMBINATION OF SOLID-ROCKET LAUNCH VEHICLE AND PAYLOAD DURING A GROUND FIRING AND LAUNCHING	December 1975
	6 Performing Organization Code
7 Author(s)	8 Performing Organization Report No
James A. Schoenster and Harold B. Pierce	L-10399
	10 Work Unit No
9 Performing Organization Name and Address	505-02-21-04
NASA Langley Research Center Hampton, Va. 23665	11 Contract or Grant No
	13 Type of Report and Period Covered
12 Sponsoring Agency Name and Address	Technical Note
National Aeronautics and Space Administration Washington, D.C. 20546	14 Sponsoring Agency Code

15 Supplementary Notes

16 Abstract

This report presents the results of a study into the environmental vibrations of a payload mounted on a rocket launch vehicle (Nike). Data were obtained during the flight acceptance test of the payload, the firing of the total vehicle in a unique test stand, and the powered and unpowered flight of the vehicle. The vibrational response of the structure was measured. Data were also obtained on the fluctuating pressures on the outside surface of the vehicle and inside the forward and aft ends of the rocket chamber. A comparison of the data from the three test conditions indicated that external pressure fluctuations were the major source of vibrations in the payload area. Pressure fluctuations within the rocket motor were the major source of vibrations contiguous to the payload.

17 Key Words (Suggested by Author(s))	18 Distribution Statement
Environmental vibrations Payload vibrations Rocket test stand Solid-rocket launch vehicle	Unclassified – Unlimited Subject Category 18

19 Security Classif (of this report)	20 Security Classif (of this page)	21 No of Pages	22 Price*
Unclassified	Unclassified	35	$3.75

*For sale by the National Technical Information Service, Springfield, Virginia 22161

COMPARISON OF VIBRATIONS OF A COMBINATION OF SOLID-ROCKET LAUNCH VEHICLE AND PAYLOAD DURING A GROUND FIRING AND LAUNCHING

James A. Schoenster and Harold B. Pierce
Langley Research Center

SUMMARY

This report presents the results of a study of the environmental vibrations of a payload mounted on a rocket launch vehicle during launch. A special payload designed for obtaining vibrational measurements was mounted on a Nike rocket motor. Data were obtained during the flight of the vehicle, the firing of the identically configured vehicle in a unique ground test stand, and the flight acceptance test of the payload. Comparisons of power spectral density plots from each condition were made to determine the sources and levels of vibration. Data collected included the vibratory response of the structure at several locations, measurements of the fluctuating pressures in the forward and aft ends of the rocket motor, and the fluctuating pressures on the surface of the payload. Results of these comparisons indicated that external fluctuating pressures on the surface of the vehicle were the major source of vibration in the forward end of the payload. However, the internal fluctuating pressures in the rocket motor contributed to the vibration levels throughout the vehicle and were the major input to the structure contiguous to the motor. Because the external pressures were a significant source of vibration, the structure continued to vibrate at significant levels during flight after the rocket motor burnout.

INTRODUCTION

In the development of spacecraft payloads, much effort is required to determine the dynamic loads to which the payload is subjected during launch and to determine the ability of the spacecraft to withstand these loads. Because of the complex nature of the dynamic loads, particularly in the vibration environment, the most common method of determining the reliability of the payload is to test it. Problems associated with such testing involve undertesting, overtesting, and determining the proper method of simulating the environment. Undertesting could result in missed problems which appear only at higher levels. Overtesting could cause overdesign which might cost both time and money and could impose excessive weight penalties. The problem of the proper method of simulation involves such questions as whether acoustic or direct mechanical vibration excitation is

preferred or whether both methods of simulation are necessary. Many studies, both analytical and experimental, have been conducted to predict the vibration environment for the complex payloads carried on large launch vehicles (refs. 1 and 2), and large facilities are used to perform these tests. In addition, some studies have been conducted to evaluate the effectiveness of the environmental studies (ref. 3). While the cost of such methods of testing represents only a fraction of the money spent to develop large payloads, it still represents a large investment in terms of absolute effort. Generally, this effort is far too costly for the development of small payloads such as those used on sounding rockets. Payloads are qualified to some general specification and, because there is a significant lack of data to support these specifications, the tests are not necessarily representative of the flight conditions. Some data have been obtained on specific vehicles, but the unique characteristics of the rocket motor limit the applicability of these data to all vehicles (ref. 4). In some situations additional firings are conducted to obtain the environmental data and to check out the reliability of the system (ref. 5). However, most of these small rocket payloads depend on general specifications designed to cover all situations.

A program to investigate the source and magnitude of vibrations in payloads when using small solid rockets has been conducted at the Langley Research Center. As part of this program, experimental data on a typical payload-launch-vehicle combination were obtained during both a flight and a ground firing of the vehicle. A unique test stand which allowed the vehicle to vibrate freely while restricting the forward motion of the vehicle (thereby eliminating any effects of this motion) was developed for the ground firing experiments. Preliminary results on the firing of a Nike rocket with a dummy payload in this test stand were presented in reference 6. To aid in understanding the vibration behavior of a solid-rocket motor, data on the fluctuating pressures and vibrations of a Nike rocket motor when fired against a hard backstop were obtained and reported in reference 7. In continuing this program, a payload was designed representing typical small rocket equipment. The payload, which incorporated a data acquisition system for recording the fluctuating data, was mounted on a Nike rocket and fired in the test stand. To obtain comparison data, the identical configuration was then launched from the NASA Wallops Flight Center. Data were obtained during both firings on the vibrational response of the payload and on the fluctuating pressures within the rocket motor and upon the surface of the nose cone.

This report presents the results of the test-stand firing, of the flight, and of the flight acceptance test of the payload. Comparisons of the data between these different environmental conditions are made to aid in the understanding of the vibrational forcing functions and the responses of the payload. These results include vibration levels, fluctuating pressures in the engine and on the surface of the nose cone, and the resulting structural response. Comparisons between the flight responses, the test-stand responses, and

the acceptance test responses are made. These comparisons are presented as time histories and power spectral densities of the measurements. Measurements are given in SI and U.S. Customary Units. Values were obtained in U.S. Customary Units.

TEST VEHICLE DESCRIPTION

The test vehicle consisted of two major sections: a payload and a launch vehicle (fig. 1). The overall vehicle weighed 705 kg (1554 lbm) and was 5.408 m (212.9 in.) long.

Launch Vehicle

The launch vehicle was a single-stage, fin stabilized booster consisting of a Nike solid-rocket motor, type M88, with a 0.255-m^2 (2.75-ft^2) fin assembly and an external pod recovery system. The rocket motor, with a diameter of 41.9 cm (16.5 in.), was 3.423 m (134.8 in.) from thrust face to nozzle exit. The motor weighed 542.0 kg (1195 lbm), had a nominal thrust of 200 kN (45 000 lbf), and had a nominal burn time of 3.2 seconds. The total mass of the launch vehicle was 624 kg (1376 lbm). A Nike motor identical to the one used in the test stand was used for the flight. The propellants for the test-stand firing and the flight were selected from the same manufacturing lot. Since the ground test vehicle is mounted upside down in the test stand, a modification was made to the motor to hold the propellant in place during firing. This modification was also included in the flight motor. The standard rocket motor has a conical spring holding the propellant against the aft end of the case with a force of about 2.9 kN (650 lbf). Many small springs were added around the edge of the propellant to increase this force to 9.8 kN (2210 lbf).

Payload

The payload consisted of an instrument section, a recovery section, and an adapter section. An ogive-shaped nose cone covered the instrument section. The forward instrument post held the flight tape recorder and some of the experimental-instrumentation electronics. As a protective measure this post was mounted on vibration isolators to reduce the transmission of vibrational forces to the flight tape recorder. The total mass of the isolated post was 11 kg (24 lbm). The aft instrument post held the flight accelerometer, a lateral vibrometer, and a longitudinal vibrometer. These two parts formed the instrument section and were enclosed in a moisture-proof shell. The instrument section weighed 15 kg (32 lbm) and was 69.1 cm (27.2 in.) long.

The recovery section consisted primarily of a structure to house the payload recovery parachute system. The recovery section weighed 33 kg (72 lbm) and was 68.3 cm (26.9 in.) long.

The adapter section provided the interstage structure which attached the instrument and recovery sections to the launch vehicle; this section also housed such items as vehicle batteries, programer, vehicle instrumentation, and umbilical connectors. The adapter section weighed 34 kg (74 lbm) and was 61 cm (24.0 in.) long.

TEST CONDITIONS

The payload was subjected to three different tests in the following sequence: (1) a flight acceptance test, (2) a test-stand firing using a rocket motor, and (3) a flight test on a rocket motor. Instrumentation was placed at the same location for each of these tests.

Flight Acceptance Test

The payload was mounted on a 44.5-kN (10 000-lbf) shaker (fig. 2) and subjected to the vibration environment shown in table I. The aft end of the adapter was bolted to a flat aluminum plate 50.8 cm (20 in.) in diameter and about 5 cm (2 in.) thick. The plate weighed 29.3 kg (64.5 lbm). During the random vibration test along the thrust axis of the launch vehicle, data were recorded from vibrometers on the flight record system.

Test-Stand Firing

The test vehicle, including the rocket motor and payload but not the fins, was mounted with the exhaust going vertically upward in a test stand. A torsion bar system absorbed the energy of the thrust and limited the overall displacement of the vehicle while allowing it to vibrate freely. The fundamental natural frequency of the fully loaded rocket vehicle suspended in the test stand was about 6 Hz. Shown in figure 3 is the test stand with a Nike launch vehicle and a simulated payload. Additional details on this stand may be found in reference 6.

Flight

The test vehicle was launched from a rail launcher (fig. 4) at an effective launch elevation angle of 80°. Data from the transducers were recorded on an on-board flight tape recorder for the initial 45 seconds, a period which included the 3.6 seconds of powered flight. After the payload and launch vehicle separated and a recovery chute deployed, the payload was recovered using standard air-to-air recovery techniques.

INSTRUMENTATION AND DATA ANALYSIS

Instrumentation

The transducers were located at the same locations for each of the test conditions. The approximate locations of each of the transducers are shown in figure 1. Types of

measurements and the linear operating range of each of the measuring systems are presented in table II. Shown in figures 5 to 10 are photographs of the actual installations except for the acoustic transducers. These transducers were flush mounted on the surface of the payload. One was mounted on the recovery section, and one was mounted on the adapter section. The transducers were separated by a distance of about 67.9 cm (26.75 in.). In some of these figures more than one transducer is shown; however, only the flight transducer is identified. The duplicate transducers were mounted only during the ground test for comparison checks with the flight record system. All but one of the vibrometers measured vibrations along the longitudinal axis of the vehicle. Only one vibrometer mounted on the aft instrument post was oriented in the lateral direction; therefore, in this report, that vibrometer is the only transducer which carries an orientation notation. A list of photographs showing the installation of the transducers inside the vehicle follows. The arrows in the figures point to the transducer.

Data from all flight transducers were obtained during the test-stand firing and the launching. Data from only the vibrometers in the instrumentation and adapter sections were obtained during the flight acceptance tests.

Data Analysis Techniques

Oscillograph traces of all the data were made to obtain preliminary evaluations. Peak values and time durations were obtained from these records and are reported for the "steady-state" data such as overall motor pressure and vehicle acceleration. Time periods of significant fluctuating data were selected from these records and power spectral density analyses were made (ref. 8). Data are presented in the form of power spectral densities for comparison purposes. Because the properties of the vehicle were not constant (i.e., the mass loss caused by propellant combustion) and because the data were limited in time duration, a compromise between frequency resolution and statistical accuracy was necessary. A check of the major vehicle vibrational modes indicated that these frequencies did not vary more than about 40 Hz between the vehicle without grain and a fully loaded vehicle. Therefore, the concept of "self-stationarity" (refs. 6 and 8) was used and a stationary analysis was performed. A review of the oscillograph traces indicated that time periods of 1.6 seconds could be obtained for analysis. Combining these

time elements with the 40-Hz bandwidth resulted in 128 statistical degrees of freedom. The upper frequency limit of 5000 Hz was determined by the instrumentation system limitations.

RESULTS AND DISCUSSION

The results from this investigation are presented in figures 11 to 14. Oscillograph plots of both the flight and test-stand measurements (figs. 11 and 12) were used to provide a qualitative evaluation of the data. These plots were also used to aid in selecting specific time periods for vibration and pressure power spectral-density analyses. Comparisons of these analyses for powered flight, test-stand firing, and analyses of the flight acceptance test (FAT) data are presented in figure 13 and are discussed in this section. Comparisons of these analyses for the powered and unpowered flight conditions are presented in figure 14 and are also discussed in this section. These comparisons are then evaluated for trends and conclusions resulting from this study.

Qualitative Evaluation of Data

The vehicle performance during flight is indicated by the total motor pressure and the vehicle acceleration signals (fig. 11). The total pressure reached a maximum value of 8.4 MPa (1220 psi), a value which is about 14 percent higher than a nominal value of 7.3-MPa (1058-psi) chamber pressure. The vehicle increased in acceleration to a maximum value of 37g units which occurred at 2.6 seconds burn time. Engine burnout occurred at 3.6 seconds as indicated by the change in the motor headcap pressure curve as it moves from a relatively sharp negative slope to a considerably flatter negative slope. The initial shock of ignition caused the vibrometer system to overload. However, as shown in figure 11, all vibrometers recovered to within their operational range in less than 0.2 second. Although they are not visible from the small scale used in figure 11, the longitudinal vibration levels at the instrument post, aft instrument post, forward motor ring, and the lateral vibration levels at the aft instrument post were of measurable quantities after burnout as well as during powered flight. The data from the vibrometer located on the aft motor ring became very erratic prior to burnout and were not considered to be of any value after that time. The fluctuating pressures (measured by acoustic sensors) on the adapter-section surface and on the recovery-section surface decreased slightly in overall level until Mach 1 at 1.2 seconds. At that time the transducers were severely overloaded, and a low-frequency signal appeared. However, this signal was probably caused by the overload and was not a significant measurement. A similar overload occurred prior to engine burnout; again a low-frequency oscillation occurred. The transducers recovered and appeared to be functioning satisfactorily 4 seconds after ignition. The fluctuating pressures in the motor at the nozzle and at the headcap decay from a maximum overall level

after ignition (about 0.1 sec) to a very low level (about 2.6 sec). It may be noted that these fluctuations decreased significantly prior to the static pressure peak (2.6 sec).

The transient input caused by transition through Mach 1 had almost no effect on the vibrometers (only a slight peak on some of the traces) and no effect on the fluctuating pressures in the engine. A transient phenomenon prior to burnout has a noticeable effect on all the vibrometers for a period of about 0.75 second. Based on these observations, two time periods were selected for vibrational analysis using the statistical parameters outlined in the section on data analysis. The first time period selected during powered flight ranged from 0.2 second to 1.8 seconds; this period includes transition through Mach 1. During this time period no apparent effect was seen on the vibrometer measurements. However, the surface fluctuating pressures show a high-magnitude, low-frequency signal which may not be representative of the actual loads. The second time period selected during unpowered flight ranged from 4 to 5.6 seconds; this period shows no extraneous effects on the vibration environment. Analysis of the fluctuating-pressure data is only relative in this report since the oscillograph records show that for the time periods analyzed the data are not stationary.

The data from the test-stand firing are given in figure 12 and show that the vibration in the vehicle stops at the end of rocket burning. In addition, the fluctuating pressures on the exterior surfaces of the vehicle also stop when the rocket burns out. The pressures on the exterior surface significantly exceeded the capabilities of the instrumentation system; this overload is shown by the relatively level amplitude of the peaks in the pressure. The fluctuating pressures in the motor are similar in shape to those measured in flight although the nozzle pressure appears to decay by 1.6 seconds, a full second sooner than that measured in flight. This difference in decay time is not apparent at the headcap. The low-frequency oscillation in the vibrometer traces is a natural frequency of the test stand (ref. 6).

Comparing the test-stand firing data to the flight data shows that vibrations of the vehicle in the test stand last for a considerably shorter period of time and at a higher level than do those vibrations during flight. The fluctuating pressures (acoustic sensor) on the surface of the vehicle in the test stand are considerably higher than those in flight. The fluctuating motor pressures in the rocket motor appear to be similar during both the test-stand firing and the flight.

Power Spectral Density (PSD) of Powered Flight, Test-Stand Firing, and FAT Data

Vibrometer, instrument post.- The isolation system for the instrument post appeared to function satisfactorily during flight. (See fig. 13(a).) Vibration levels peaked at about

8×10^{-4} g^2/Hz and a frequency of 140 Hz; this frequency is somewhat above the isolation-system design resonant frequency of 90 Hz. The levels at all other frequencies are considerably less. Above 500 Hz the levels never exceed 2×10^{-5} g^2/Hz, a reduction of greater than 16 dB from the peak. In contrast, this isolation did not occur during the test-stand firing. Although a peak in the PSD curve occurs at about 140 Hz, there are other frequencies at which the level exceeds 2×10^{-3} g^2/Hz; this point is an increased level of more than 2 dB over that level at 140 Hz. Data from FAT demonstrated that when the vibration is transmitted through the structure to the instrument post, isolation is provided. This fact is shown by the more than 30-dB reduction (from the peak vibration levels) at frequencies above 500 Hz. These results imply that although the isolator provides attenuation from the structurally transmitted loads, there was at least one other load path in the vehicle with sufficient energy to vibrate the isolated post. The relatively straight line above 1200 Hz was a limitation caused by the dynamic range of the analyzer and is only an indication that the actual levels were below this level.

Vibrometer, aft instrument post (lateral).- The maximum level during powered flight was 6×10^{-4} g^2/Hz and occurred in a frequency range of 200 to 300 Hz. (See fig. 13(b).) During the test-stand firing the levels were generally 10 dB, or more, above the flight levels, reaching a maximum of 2×10^{-2} g^2/Hz both at 180 Hz and at 1580 Hz. The maximum level during FAT's was 3.3×10^{-3} g^2/Hz and occurred at 1180 Hz. Although some peaks in the PSD curves may be matched for all three conditions (i.e., the response at 820 Hz), these curves do not resemble each other in any significant manner. The levels obtained during the test-stand firing exceeded those measured during flight at all frequencies; with only a few exceptions, the test-stand levels also exceed FAT level.

Vibrometer, aft instrument post.- The maximum level during powered flight was 1.8×10^{-3} g^2/Hz and occurred at a frequency of 860 Hz. (See fig. 13(c).) During the test-stand firings the levels were generally much higher than the flight levels. Above 2 kHz they were 10 dB or higher and only at 380 Hz did the flight levels exceed the test-stand levels. In addition, at 180 Hz a peak in the test-stand firing levels was about 20 dB higher than in the flight levels at that frequency. Below 2 kHz, the FAT levels ranged anywhere from 10 dB to 40 dB greater than those measured in flight and 32 dB higher to 4 dB lower than those measured during the test-stand firing. In general, there was very little similarity between the spectrum shapes for the three test conditions.

Vibrometer, forward motor ring.- The most apparent result from a comparison of flight and test-stand PSD's was their close similarity both in level and spectrum shape. (See fig. 13(d).) With one exception in the frequency range of 60 to 220 Hz, the levels of vibration were well within 4 dB of each other below 2 kHz and were generally within 10 dB up to 5 kHz. The maximum level of 3.2×10^{-3} g^2/Hz for both conditions occurred at 1580 Hz. In the frequency range of 60 to 220 Hz, the levels from the test-stand firing

were as much as 23 dB higher than those in flight. Because this location on the vehicle was very close to the control vibrometer during the FAT's, the levels varied about the 7×10^{-3} g^2/Hz controlled input and did not exhibit any similarity in level or shape to the PSD's of the flight or test-stand firing. The levels differed anywhere from 6 dB to 40 dB below 2 kHz.

Vibrometer, aft motor ring.- As was the case of the forward motor ring vibrometer, the levels and spectrum shape were very similar for the flight and test-stand firing data. (See fig. 13(e).) With the exception at 180 Hz, the levels were generally well within a 7-dB range of each other up to the 5 kHz analyzed. At 180 Hz the test-stand PSD's were 22 dB higher than those measured in flight. The maximum level was 7×10^{-3} g^2/Hz at 1540 Hz and occurred during flight. This part of the structure was not included in the FAT's, and therefore, no FAT data are available.

Fluctuating pressure, adapter section.- The fluctuating-pressure spectrum on the adapter section during the test-stand firing reached a peak value of 20 kPa^2/Hz (4.2×10^{-4} psi^2/Hz) at a frequency of 140 Hz and decayed at an approximate rate of 5 dB per octave. (See fig. 13(f).) The fluctuating-pressure spectrum during powered flight peaked at the lowest frequency analyzed, 20 Hz, and also decayed at about 5 dB per octave. However, above 500 Hz the PSD levels during flight were approximately 12 dB to 15 dB lower than those measured during the test-stand firing.

Fluctuating pressure, recovery section.- The fluctuating-pressure spectrum on the recovery section during test-stand firing and flight were very similar to the spectrum measured on the adapter section. (See fig. 13(g).) Although the peak in the spectrum (3.2 kPa^2/Hz (6.7×10^{-5} psi^2/Hz)) during the test-stand firing occurred at 260 Hz rather than 140 Hz, the shape of the spectrum is somewhat discontinuous throughout the lower frequency and may be slightly distorted. Both spectrums decayed at a rate of about 5 dB per octave, and the flight PSD levels are 8 dB to 15 dB lower than those measured during the test-stand firing.

Fluctuating pressure, nozzle.- The fluctuating-pressure spectrum at the nozzle end of the rocket motor for both the flight and the test-stand firing had similar spectral shapes and never differed by more than 5 dB over the frequency range analyzed. (See fig. 13(h).) The maximum PSD level of 0.29 MPa^2/Hz (6.1×10^{-3} psi^2/Hz) occurred at the lowest frequency analyzed, and the spectrum decayed at 0.004 dB/Hz. These values agree closely to a maximum pressure PSD of 0.11 MPa^2/Hz (2.3×10^{-3} psi^2/Hz) and a slope of 0.004 dB/Hz as shown in reference 6 for the same type rocket motor.

Fluctuating pressure, headcap.- The fluctuating-pressure spectrum at the headcap for both the flight and the test-stand firing had similar spectral shapes and never differed by more than 4 dB below 2 kHz and less than 8 dB up to 4 kHz. (See fig. (13(i).) The maximum PSD level of 15 kPa^2/Hz (3.2×10^{-4} psi^2/Hz) occurred at 1540 Hz during the

test-stand firing; during flight the maximum level was about 1 dB lower and occurred at 1500 Hz. The peak amplitude was about 7 dB higher than that reported in reference 6; however, the peak occurs in the same frequency range, and the spectrum shapes were similar.

PSD Analysis of Data During Powered and Unpowered Flight

Vibrometer, instrument post.- The PSD shapes were similar during the powered and unpowered flight conditions. (See fig. 14(a).) However, the PSD levels were slightly higher during the unpowered portion of the flight. The maximum level of 1.4×10^{-3} g^2/Hz occurred during unpowered flight and was about 2 dB higher than that measured during powered flight. In addition, above 750 Hz the PSD levels were about 10 dB higher during powered flight.

Vibrometer, aft instrument post (lateral).- The PSD shapes were similar during the powered and unpowered flight conditions. (See fig. 14(b).) Generally the PSD shapes did not differ by more than 8 dB over the frequency range analyzed.

Vibrometer, aft instrument post.- The PSD shapes were not alike and, with only a few exceptions, the levels during unpowered flight were higher than those measured during powered flight. (See fig. 14(c).) During the unpowered flight, a maximum level of 3.3×10^{-3} g^2/Hz was reached. This level was higher by 3 dB than the highest level measured during powered flight. These peaks did not occur at the same frequency. At 1580 Hz a noticeable peak was observable during powered flight. However, the peak was not as significant during unpowered flight.

Vibrometer, forward motor ring.- The PSD shapes for the powered and unpowered flight conditions were not similar. (See fig. 14(d).) Although the peak response occurred during powered flight (3.2×10^{-3} g^2/Hz), the overall response during unpowered flight was generally much higher, as much as 30 dB at frequencies about 3620 Hz. During the unpowered flight the PSD levels reached a maximum of 7.9×10^{-4} g^2/Hz with several peaks within 2 dB of that value.

Fluctuating pressure, adapter section.- The PSD curves for both the powered and unpowered flight were similar; the only significant difference occurred at frequencies below 180 Hz. (See fig. 14(e).) The oscillograph records (fig. 11) indicate a high-amplitude signal starting about lift-off and decaying essentially to zero by Mach 1. Data for powered and unpowered flight indicated this high-amplitude signal was concentrated in the frequencies below 180 Hz. At all other frequencies the PSD curves were well within 6 dB of each other.

Fluctuating pressure, recovery section.- The PSD curves for both the powered and unpowered flight were again similar, not differing by 5 dB above 260 Hz. (See fig. 14(f).) The situation was similar to that at the adapter section, where a high-amplitude signal

starting about lift-off decayed until Mach 1. The PSD curves indicated that the high-amplitude signals were concentrated in the frequency range below 260 Hz.

Comparison of data from various test conditions.- The maximum payload vibration level measured during flight was 3.2×10^{-3} g^2/Hz and occurred during unpowered flight (fig. 14(b)). The maximum vibration level in the rocket motor was 7×10^{-3} g^2/Hz and occurred at the aft motor ring during powered flight (fig. 13(e)). In general, however, the vibration levels during unpowered flight were higher than those during powered flight (fig. 14). The vibration levels during the test-stand firing in the payload reached a maximum of 1.3×10^{-2} g^2/Hz (fig. 13(c)) and, in general, were also higher than those during powered flight, particularly above 2 kHz where the levels were always 20 dB above flight levels (figs. 13(a), 13(b), and 13(c)). The vibration levels in the rocket motor were generally well within 10 dB of each other between the powered flight and the test-stand firings (figs. 13(d) and 13(e)), with one notable exception. At about 160 Hz the test-stand firing vibration levels exceeded the launch vibration levels by more than 20 dB.

Comparison of the fluctuating pressures in the rocket motor and on the external surfaces provided a possible answer for the variation in the vibrations of the structure. The fluctuating pressures in the rocket motor did not show any obvious frequency agreement between the headcap and the nozzle. However, these pressures at their respective locations agreed well within 10 dB between the launching and ground firing (figs. 13(h) and 13(i)). Below 2 kHz the pressures were within 5 dB. Also, the fluctuating pressures on the surface of the test vehicle during the powered flight and the unpowered flight phases were well within 6 dB of each other above 200 Hz (figs. 14(e) and 14(f)). The vehicle mass after burnout (i.e., during unpowered flight) was only about 60 percent of that at the initial launch. The major difference between the test-stand firing and the powered flight (figs. 13(f) and 13(g)) was in the external fluctuating pressures on the surface of the vehicle. Because of a 160-Hz resonance response in the room in which the test stand was located, a very high external fluctuating-pressure field existed. These fluctuating pressures were 25 dB greater than those measured on the vehicle during flight. Combining the results of the powered and unpowered flight showed that the same external pressure field on the surface of the vehicle caused higher vibration levels when the vehicle weighed less and that an increased external pressure field on the same vehicle caused increased vibration levels. These effects indicate that the major source of vibration in the payload area of a vehicle using a Nike rocket is caused by the external fluctuating-pressure field.

Although the external fluctuating pressures were extremely significant in the payload area, the internal fluctuating pressures in the Nike engine also contributed to the overall levels. During rocket burning, for both the test-stand firing and the flight, a peak in the headcap pressure spectrum at about 1540 Hz to 1580 Hz (fig. 13(i)) was matched by a peak in the vibration spectrum at the forward motor ring and at the aft

instrument post (figs. 14(c) and 14(d)). During the unpowered flight period, this peak in the vibration response spectrum was not very apparent; thus, the vibration was related to the engine pressure fluctuation. In addition, the close similarity of the vibration spectra at the forward motor ring during both the test-stand firing and the powered flight (fig. 13(d)) indicated similar input forces such as those resulting from the engine pressure fluctuations. This similarity occurred even though the external pressure fluctuations (figs. 13(f) and 13(g)) were not of equal levels during these test conditions.

By comparing the data from all test conditions, the following evaluations of the test-stand simulation may be made:

(1) The ground firing did not closely simulate the actual flight conditions because of the significant contribution of the fluctuating pressures on the surface of the vehicle

(2) The vibration levels during flight were caused by a combination of external fluctuating pressures and engine fluctuating pressures

(3) The time duration of vibration during ground firing lasted only during rocket burning. However, during flight, again because of external fluctuating pressures, vibration of the structure continued for a longer period of time

(4) Both the flight data and the test-stand data indicated that a "static" firing such as that conducted in reference 7 would provide data on engine fluctuating pressures. Such data would contribute significantly to the vibration of the structure, as demonstrated by the 1540-Hz peak in the pressure spectrum.

It became apparent that the FAT method of using a shaker as a single source of input could not represent the dynamics of the flight environment either in levels or spectrum shape because of the complex nature of the vibratory input forces.

CONCLUDING REMARKS

The results of an investigation into the vibratory environment of a payload mounted on a Nike rocket launch vehicle have been presented. Data were obtained during a flight of the payload, during a firing of the rocket-payload combination in a unique test stand, and during the flight acceptance test of the payload. These data included measurements of the vibratory acceleration of the structure, the fluctuating pressures in the rocket-motor casing, and the fluctuating pressures on the exterior surface of the vehicle skin. The data were analyzed using statistical techniques and were presented as power spectral density (PSD) plots using a 40-Hz constant bandwidth filter over a frequency range of zero to 5 kHz.

The maximum level of vibration occurred during powered flight at the aft ring of the rocket motor and reached a value of 7×10^{-3} g^2/Hz. The maximum level of

vibration in the payload area occurred during unpowered flight and reached a value of 3.2×10^{-3} g^2/Hz; this value is about one-fourth the flight acceptance data (FAT) level of 1.3×10^{-2} g^2/Hz. By comparing data from the test-stand firing and the flight, it was determined that the vibrations in the vehicle were the result of a combination of inputs which included both the fluctuating pressures in the rocket case and the fluctuating pressures on the surface of the vehicle. Although it was not determined how much each of these two sources contributed, the fluctuating pressures on the vehicle surface appeared to be the more significant input to the payload. Therefore, since neither the test-stand firing nor the flight acceptance tests simulated fluctuating surface pressures, the measured vibration levels in the payload were not similar to those during flight either in spectrum shape or duration. However, it was observed that fluctuating-pressure measurements made during a "static" firing of the rocket motor would provide useful information in determining the contribution of the engine to the vibration of the vehicle.

Langley Research Center
National Aeronautics and Space Administration
Hampton, Va. 23665
October 7, 1975

REFERENCES

1. Bandgren, H. J.; and Smith, W. C.: Development and Application of Vibroacoustic Structural Data Banks in Predicting Vibration Design and Test Criteria for Rocket Vehicle Structures. NASA TN D-7159, 1973.

2. Piersol, A. G.; and Van der Laan, W. F.: A Method for Predicting Launch Vehicle Vibration Levels in the Region of the Spacecraft Adaptor. NASA CR-1227, 1969.

3. Clevenson, Sherman A.: Lunar Orbiter Flight Vibration Data and Comparisons With Environmental Specifications. NASA TN D-6006, 1970.

4. Clevenson, Sherman A.: Payload Vibration Data Measured During Five Flights of a Two-Stage Solid-Propellant Launch Vehicle. NASA TN D-963, 1962.

5. Manning, James C.: Some Flight-Induced Environmental Data Obtained From Two Sidewinder-Arcas Sounding-Rocket Launches. NASA TM X-2368, 1971.

6. Schoenster, James A.: Measurements and Analysis of Solid-Propellant-Rocket Vibrations Obtained During a Captive Flight. NASA TN D-6517, 1971.

7. Schoenster, James A.; and Pierce, Harold B.: Effects of Experimentally Measured Pressure Oscillations on the Vibration of a Solid Rocket Motor. NASA TN D-6931, 1972.

8. Bendat, Julius S.; and Piersol, Allan G.: Measurement and Analysis of Random Data. John Wiley & Sons, Inc., c.1966.

TABLE I.- FLIGHT ACCEPTANCE TEST INPUTS

[rms denotes root mean square]

Sinusoidal vibration	Random vibration
20 Hz to 30 Hz at 0.254-cm double amplitude 30 Hz to 2000 Hz at ±5g 1 sweep at 6 octaves per minute	20-Hz to 2000-Hz bandwidth 0.013 g^2/Hz (power spectral density) 5g rms overall level 15 seconds duration

TABLE II.- OPERATING RANGE OF MEASUREMENT SYSTEMS FOR TRANSDUCER

	Amplitude	Frequency, Hz
Vibrometers (Vib)	±50g	3 to 5000
Fluctuating pressure sensor (internal)	±34.4 kPa (±5 psi)	20 to 5000
Acoustic sensor (external)	2 kPa rms (0.29 psi rms)	20 to 5000
Static pressure sensor	0 to 10.3 MPa (1500 psi)	---------
Accelerometer	-10g to 60g	---------

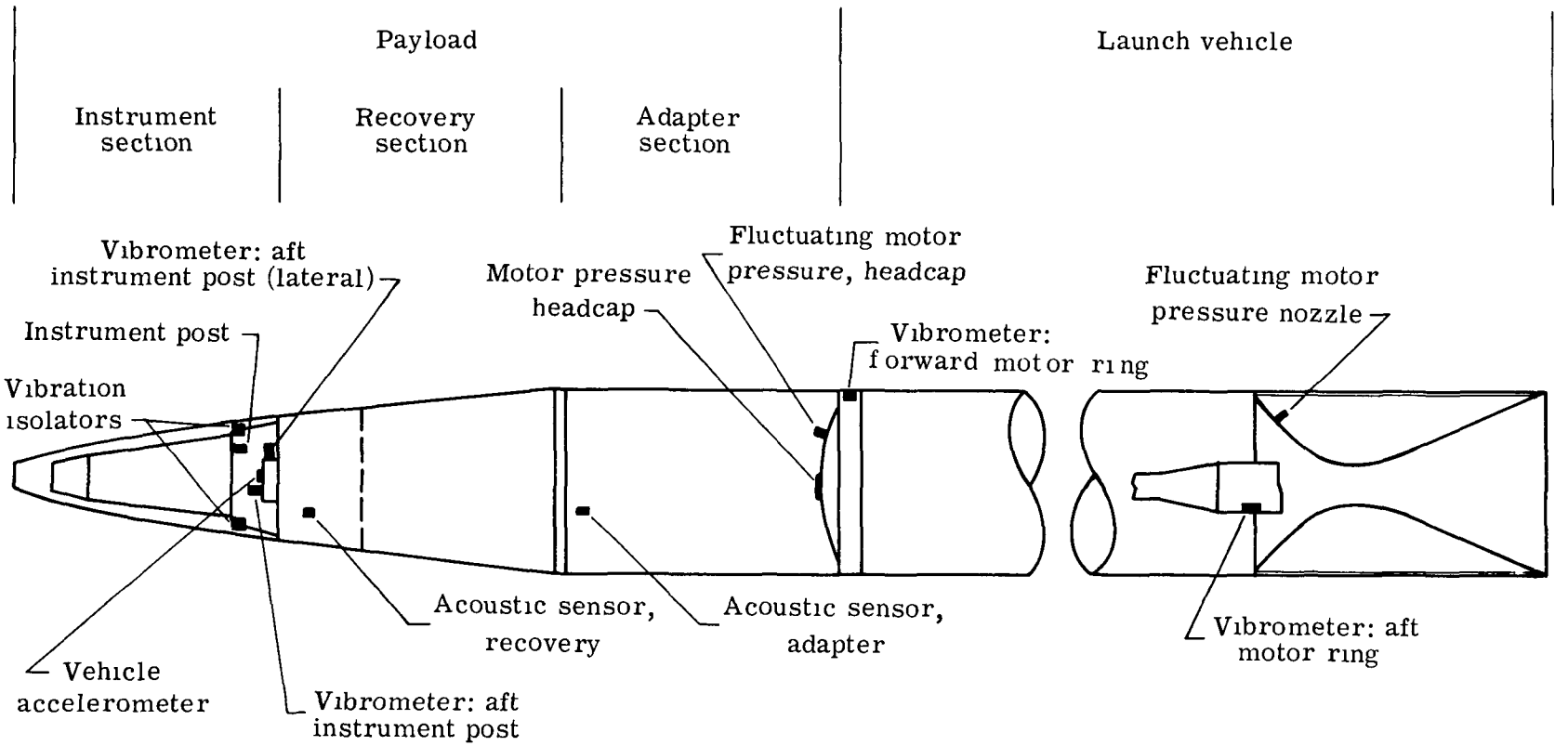

Figure 1.- Schematic of test vehicle and instrument locations (fins not shown).

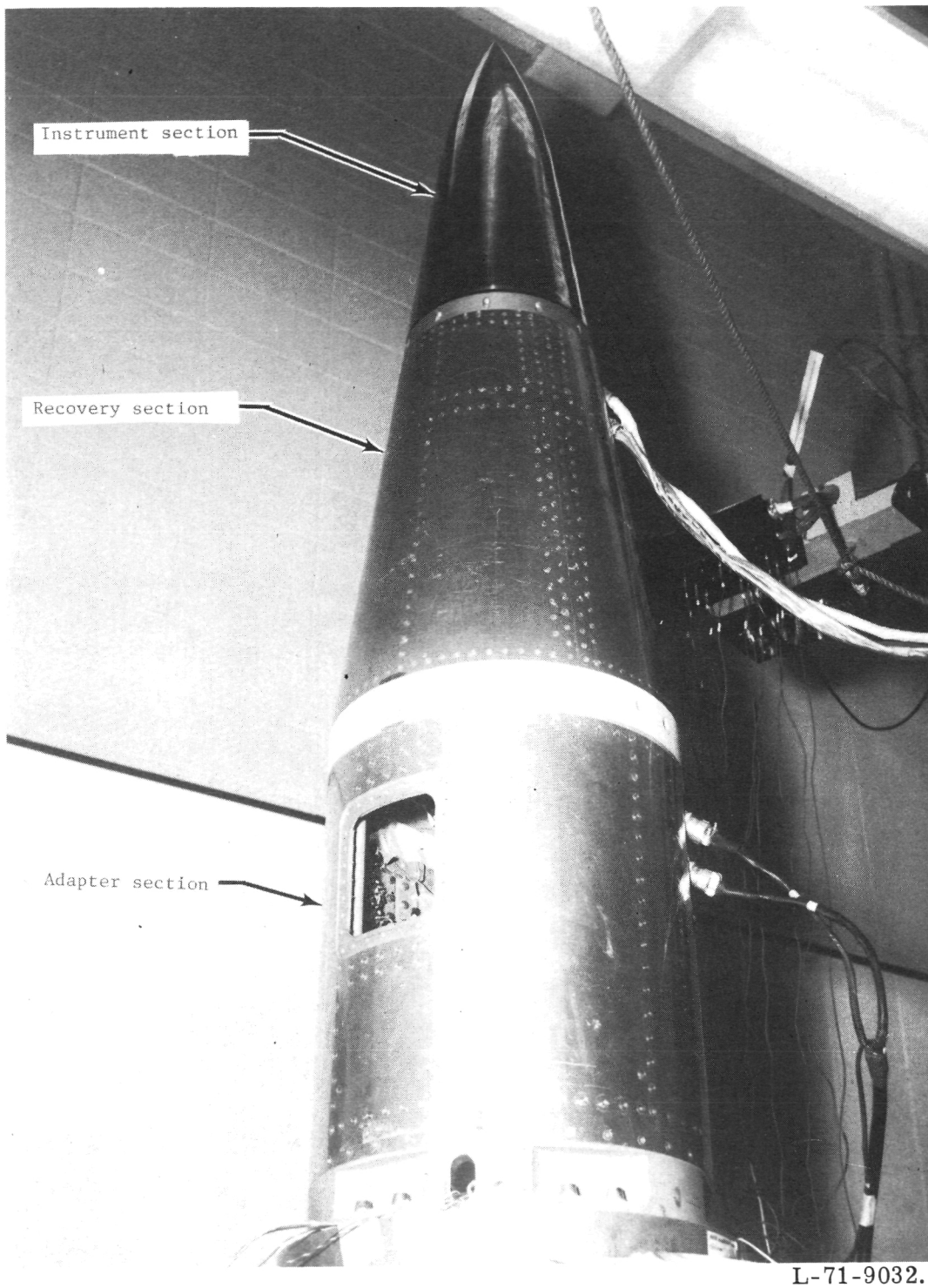

L-71-9032.1

Figure 2.- Instrument and adapter sections mounted on shaker for FAT's.

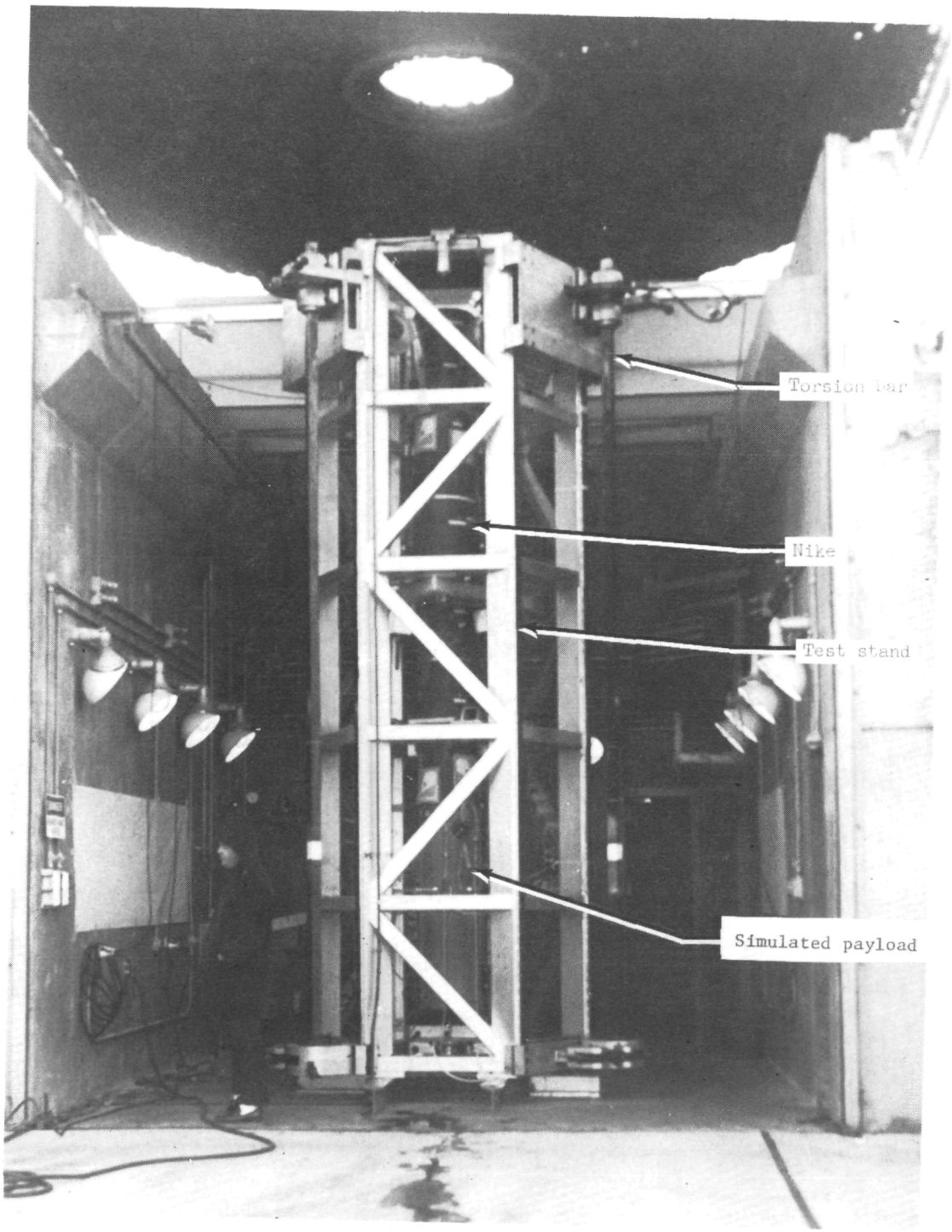

L-70-8341.2

Figure 3.- Rocket test stand and simulated test vehicle.

L-72-19

Figure 4.- Test vehicle mounted on rail launcher.

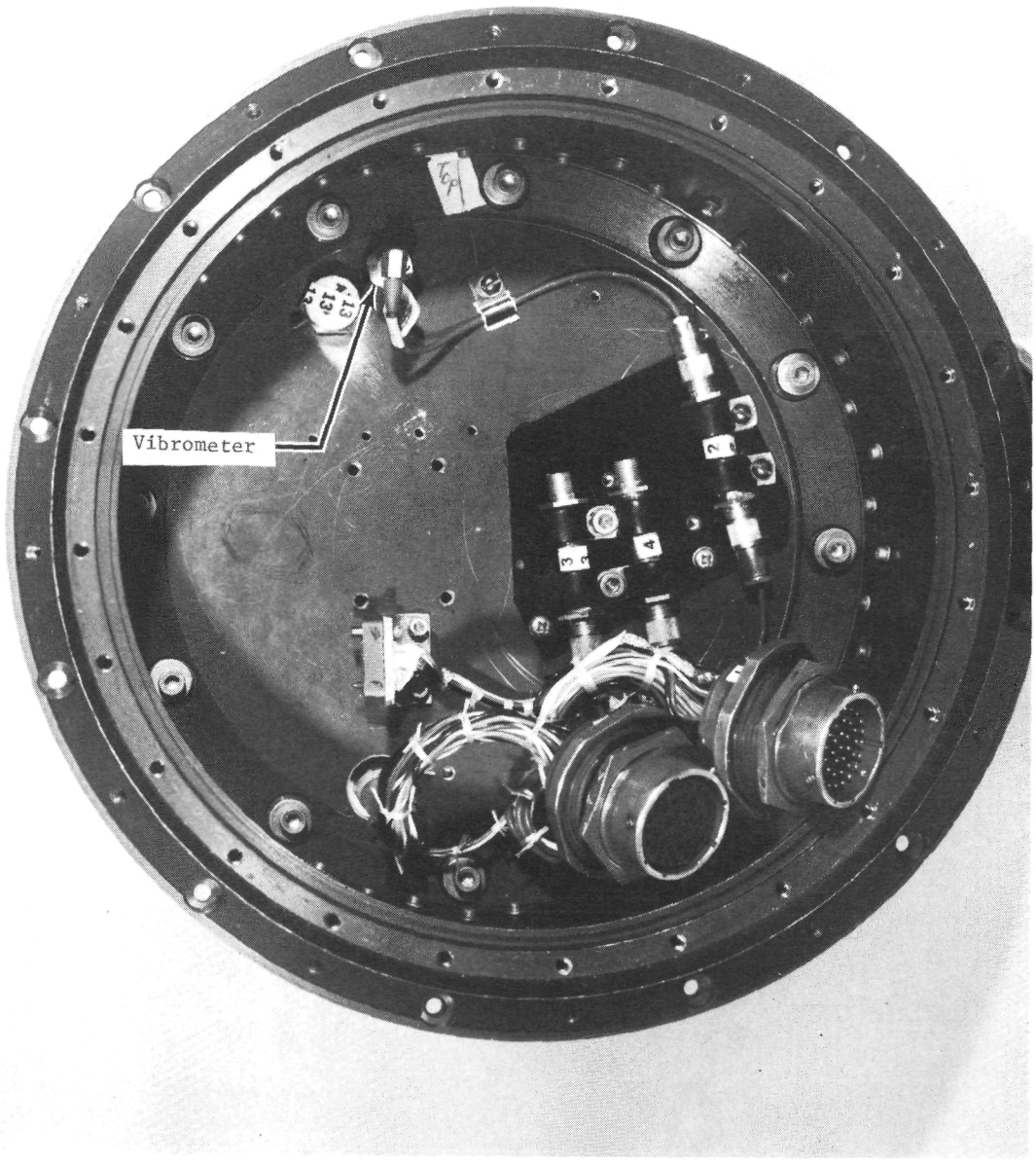

L-71-9066.1

Figure 5.- Vibrometer on forward instrument post (view looking forward).

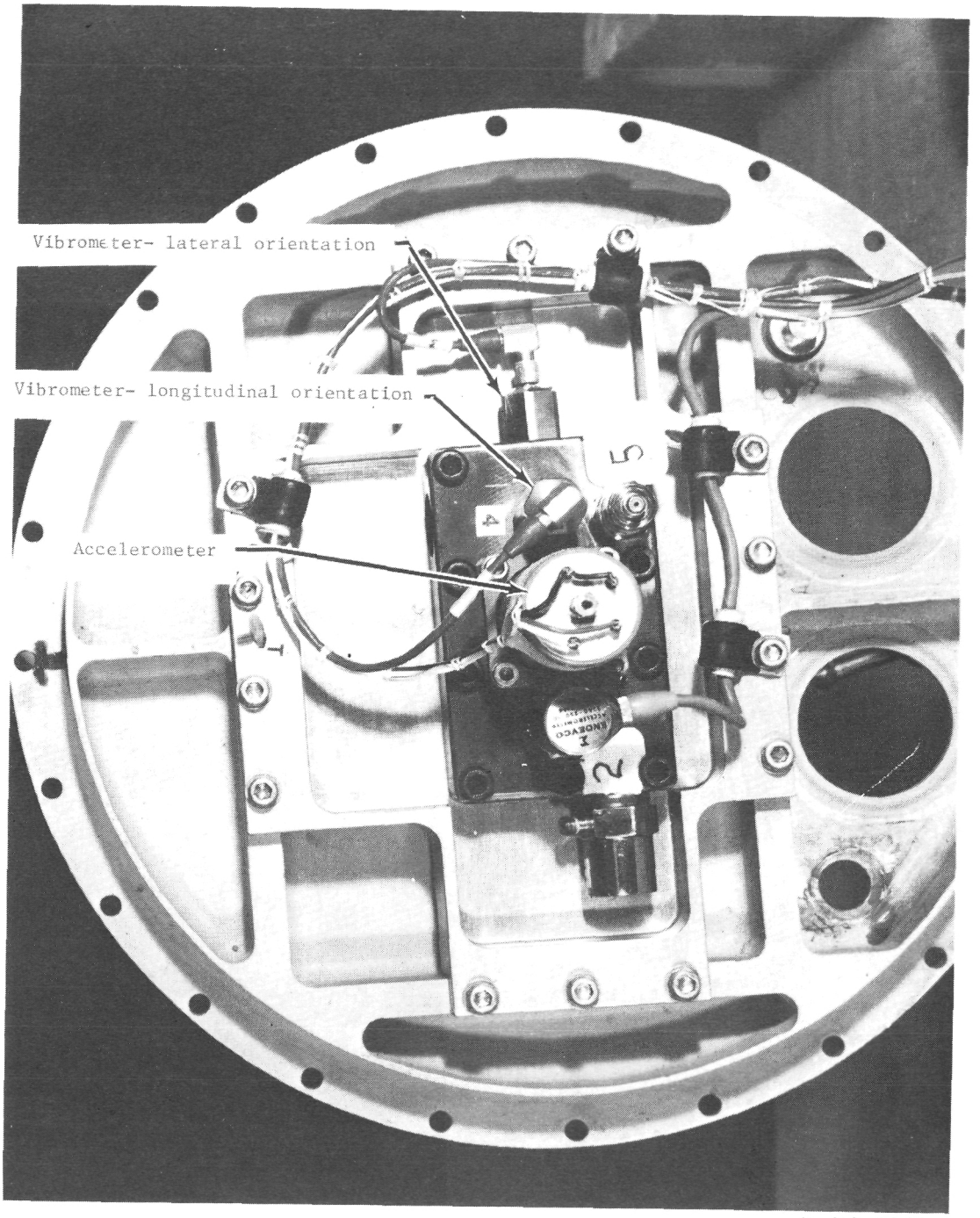

L-71-9626.1

Figure 6.- Transducer installations on aft instrument post (view looking aft).

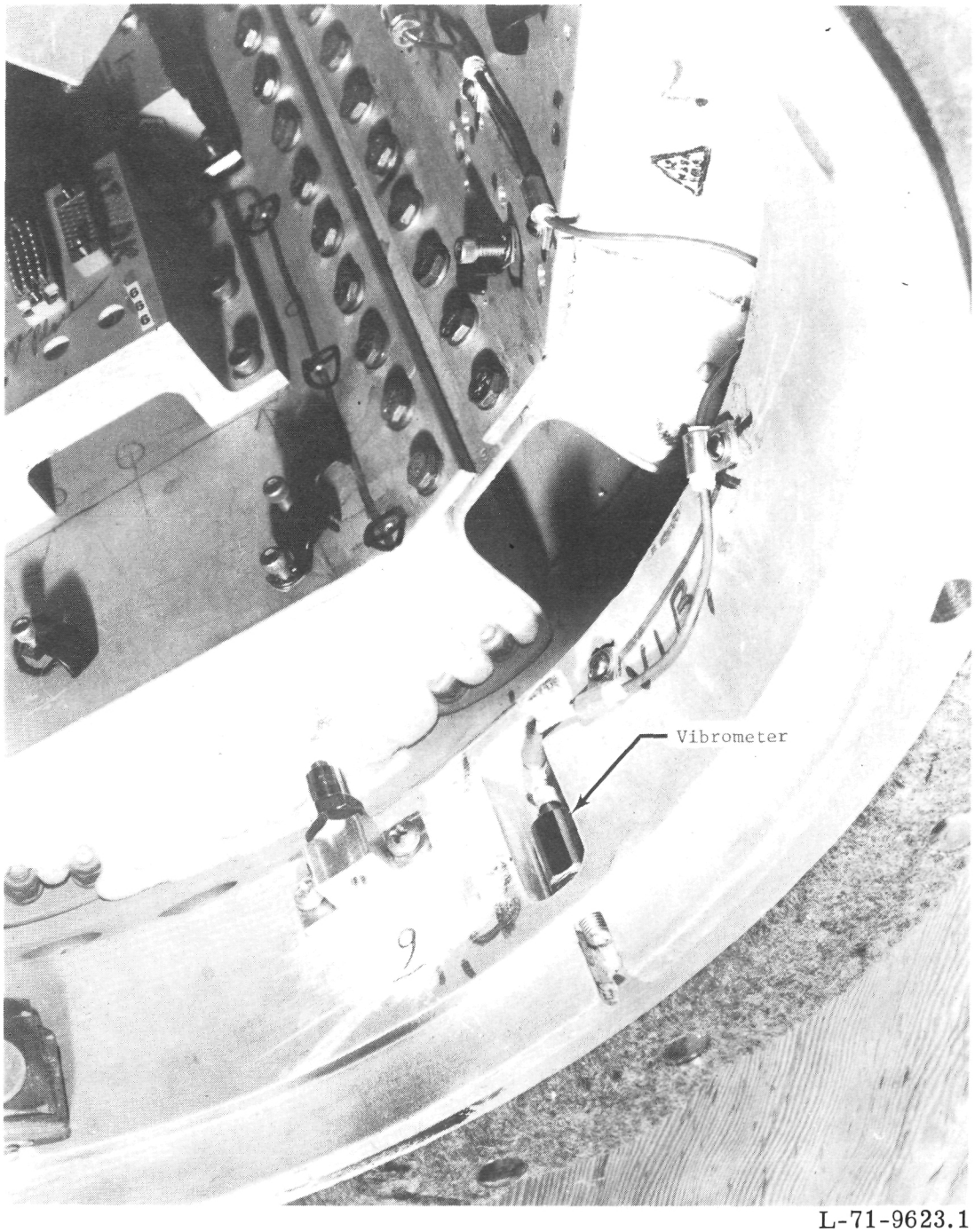

L-71-9623.1

Figure 7.- Vibrometer on forward motor ring (view looking forward).

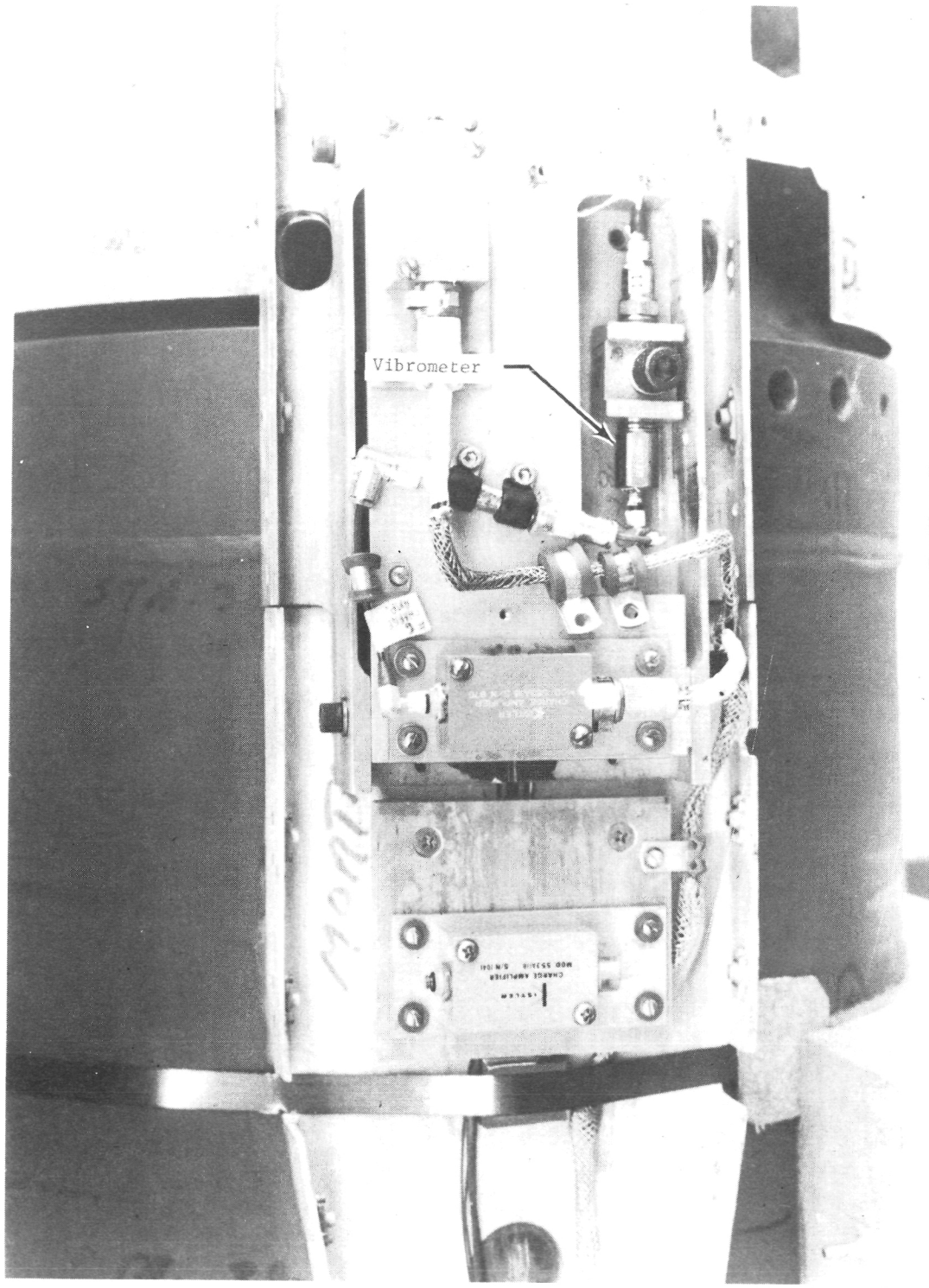

L-71-10 098.1

Figure 8.- Vibrometer on aft motor ring (side view).

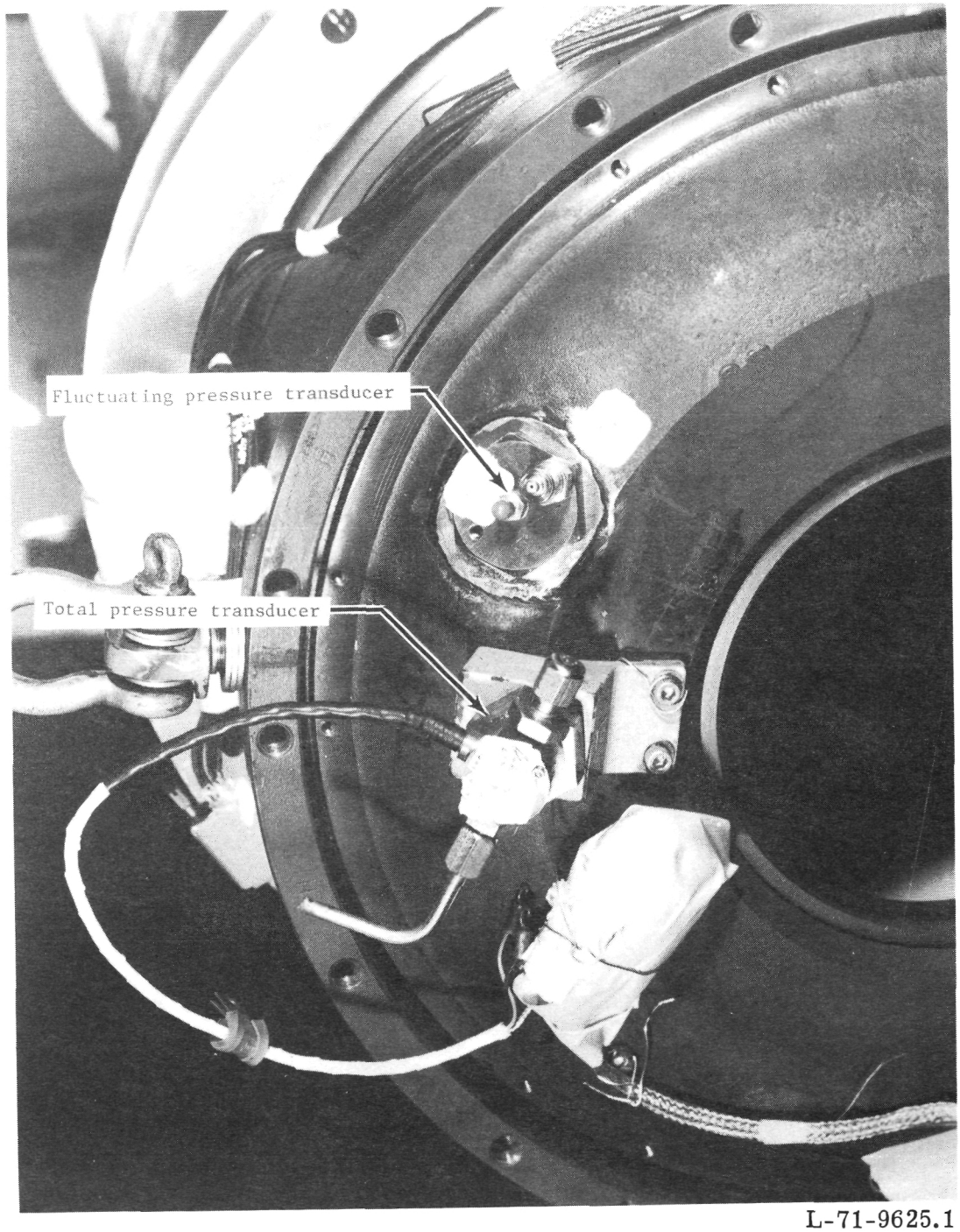

L-71-9625.1

Figure 9.- Pressure transducers on headcap of rocket motor.

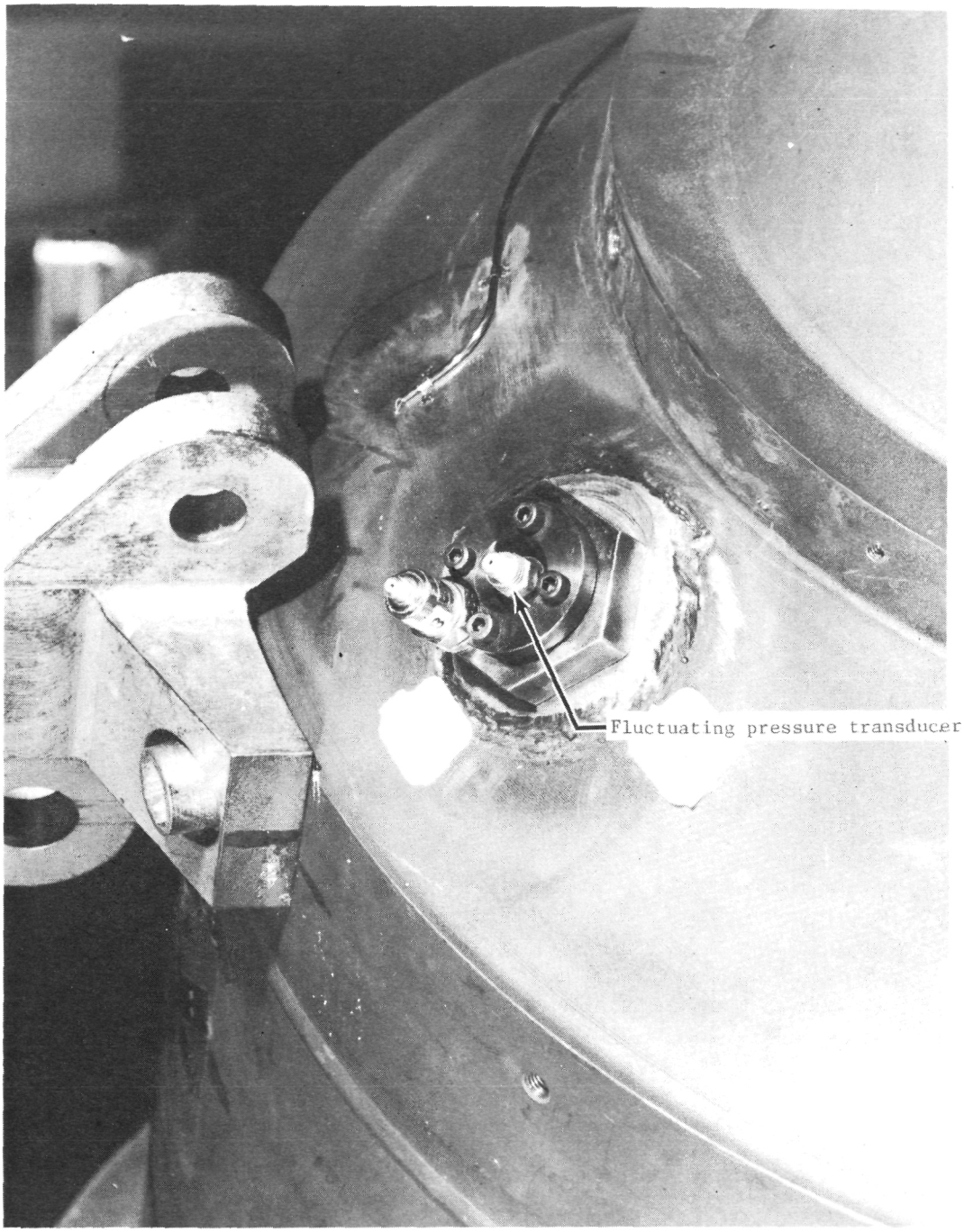

L-71-9624.1

Figure 10.- Pressure transducer on convergent section of rocket-motor nozzle.

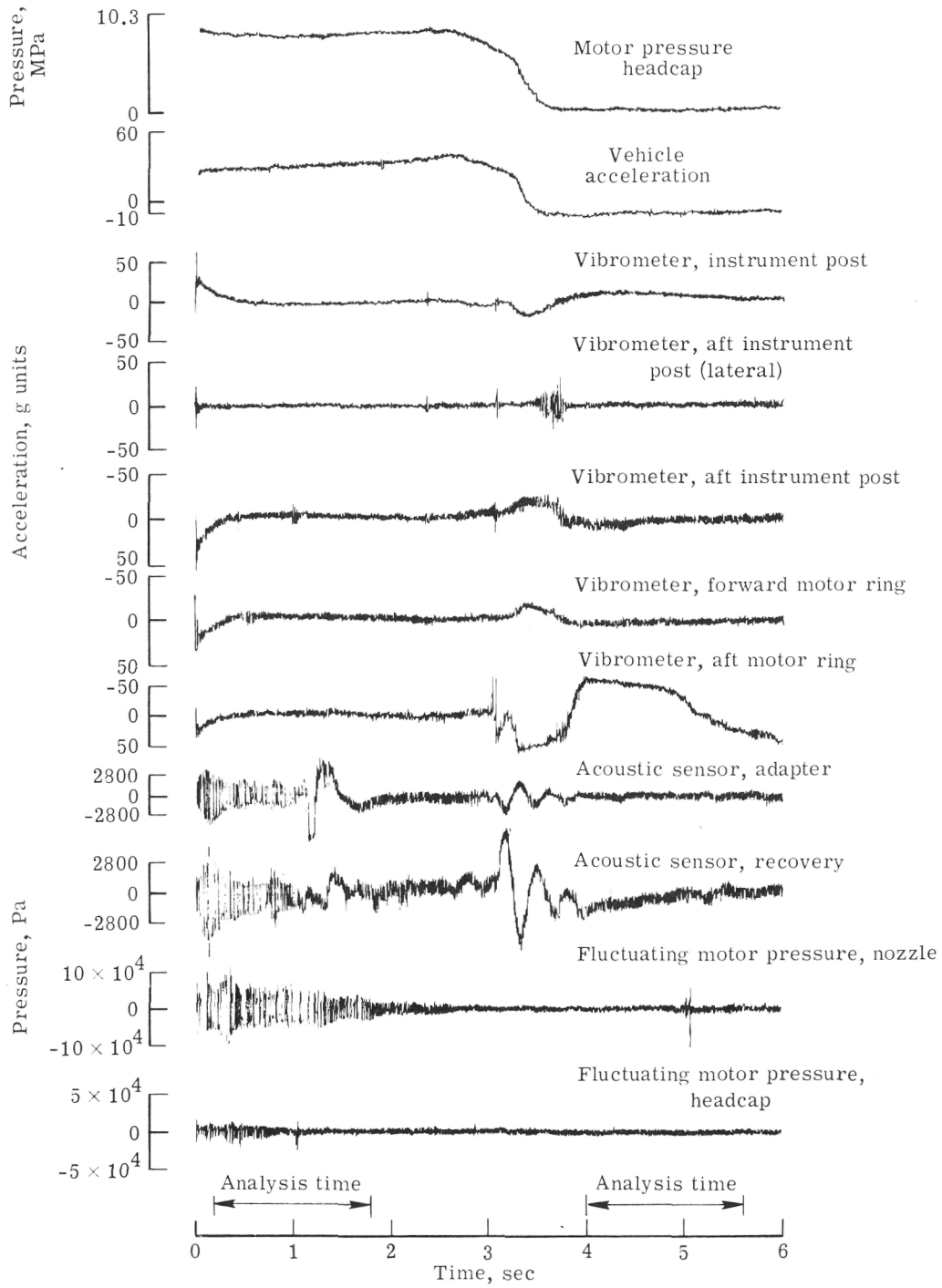

Figure 11.- Oscillograph records of rocket flight.

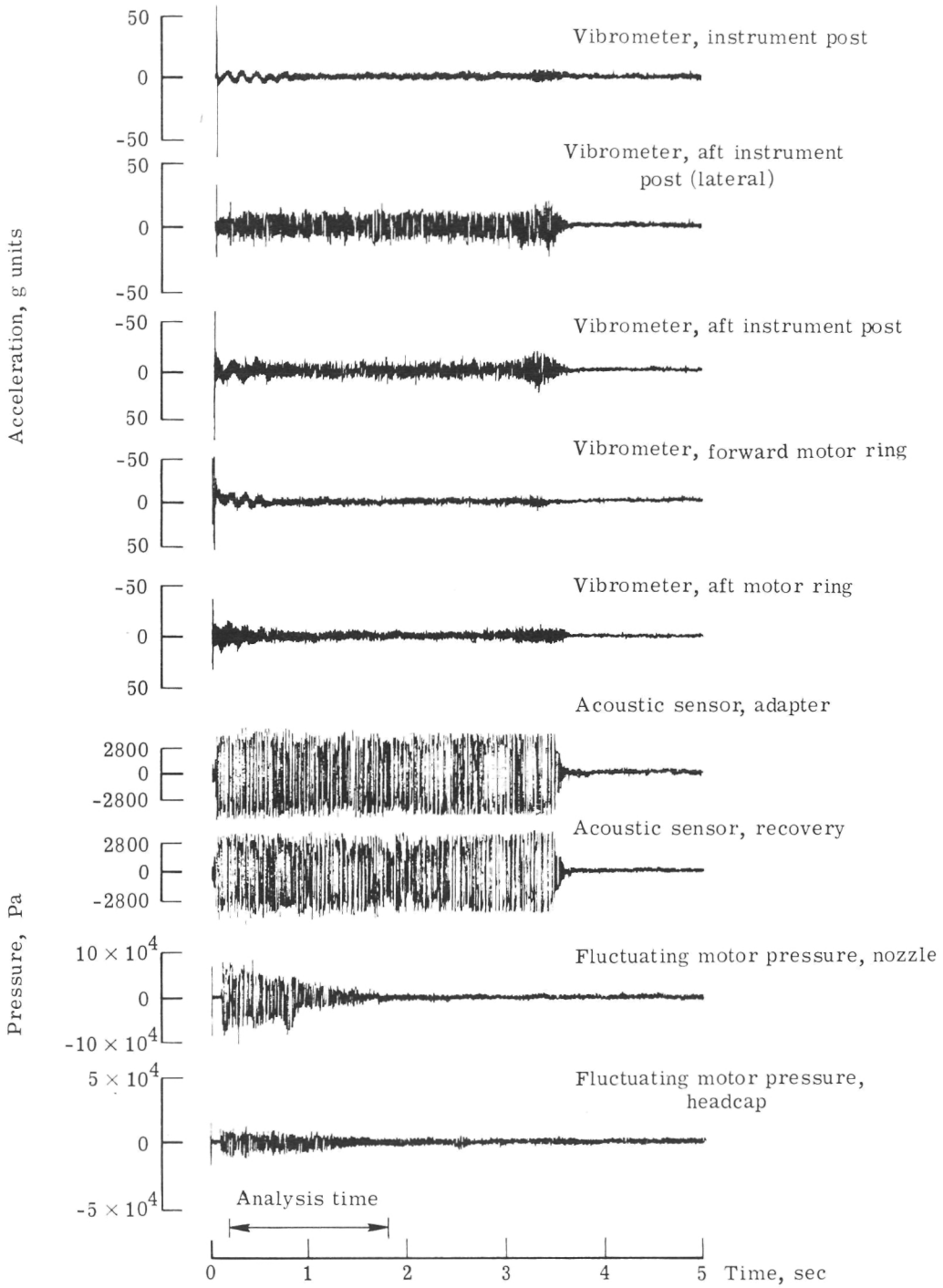

Figure 12.- Oscillograph records of tests and firing.

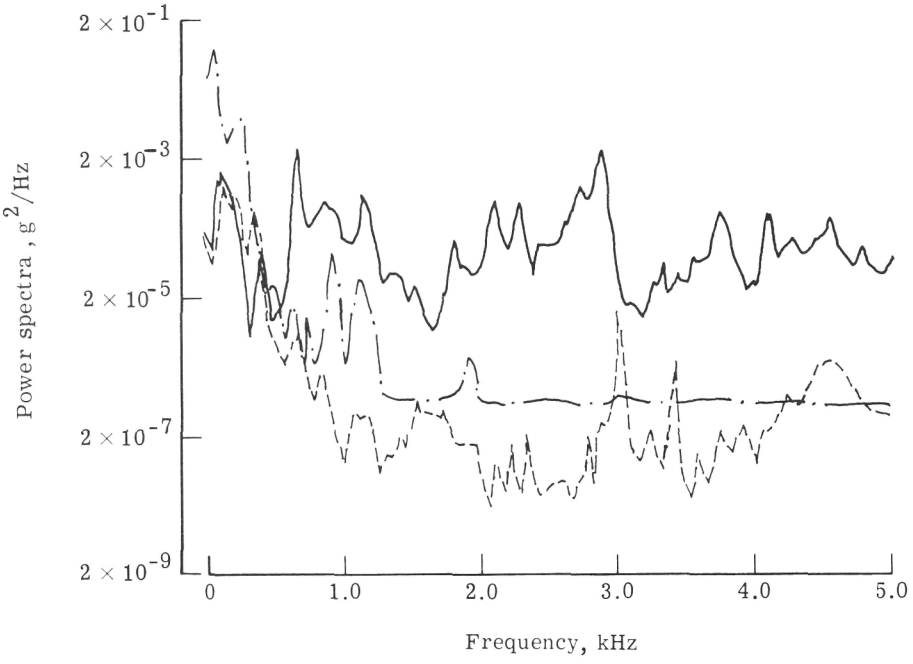

(a) Vibrometer, instrument post.

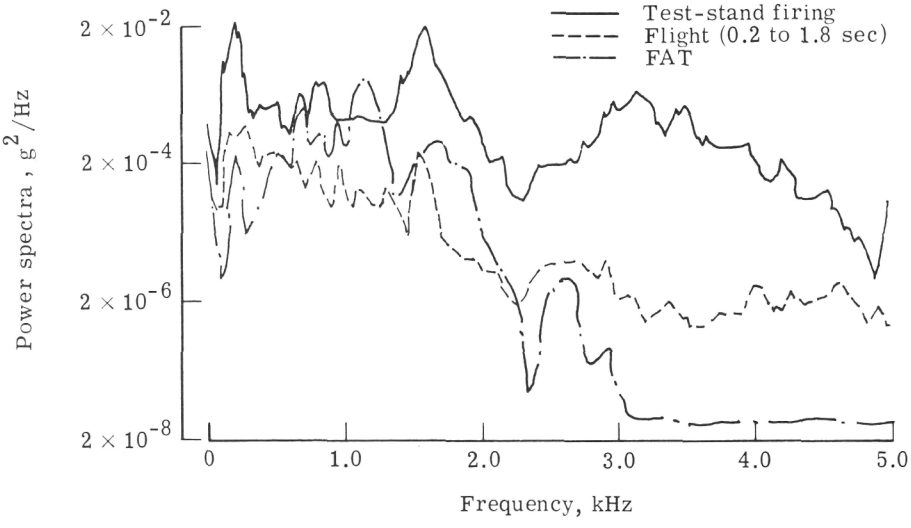

(b) Vibrometer, aft instrument post (lateral).

Figure 13.- Power spectral density analysis. Burn time, 0.2 to 1.8 sec; 40-Hz bandwidth.

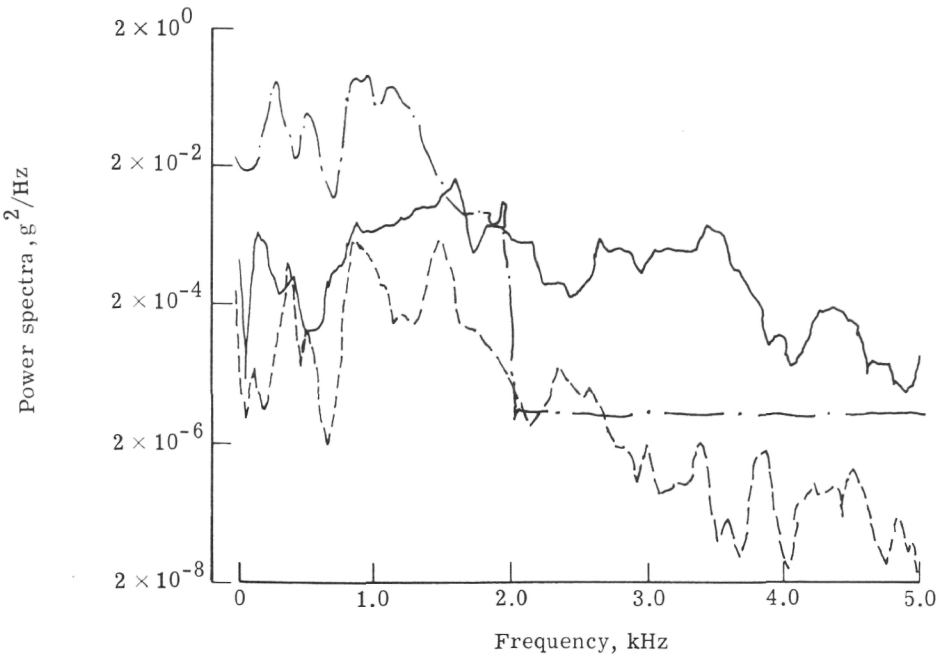

(c) Vibrometer, aft instrument post.

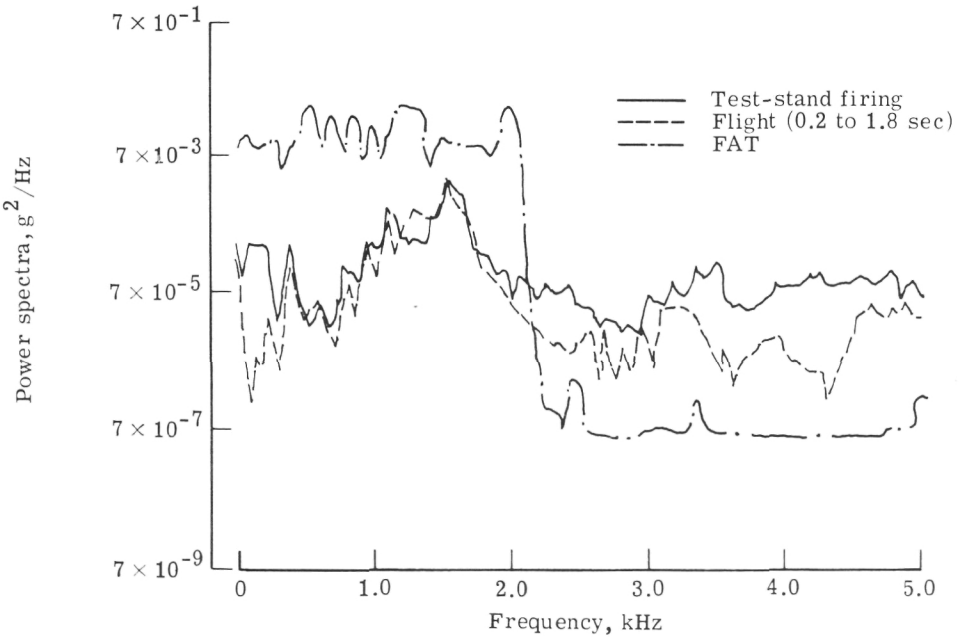

(d) Vibrometer, forward motor ring.

Figure 13.- Continued.

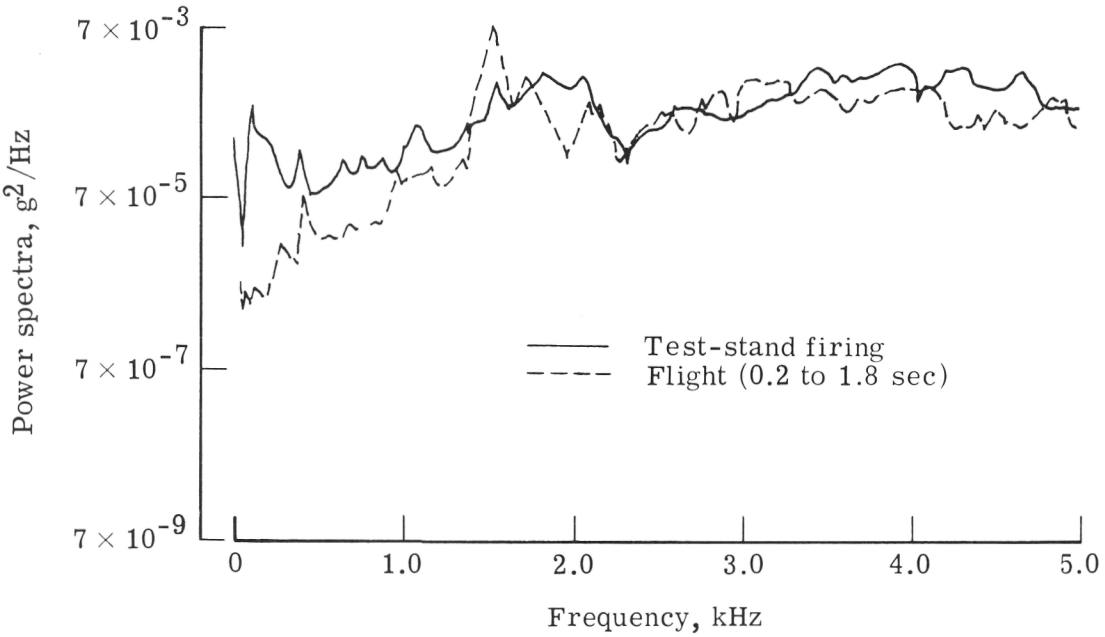

(e) Vibrometer, aft motor ring.

Figure 13.- Continued.

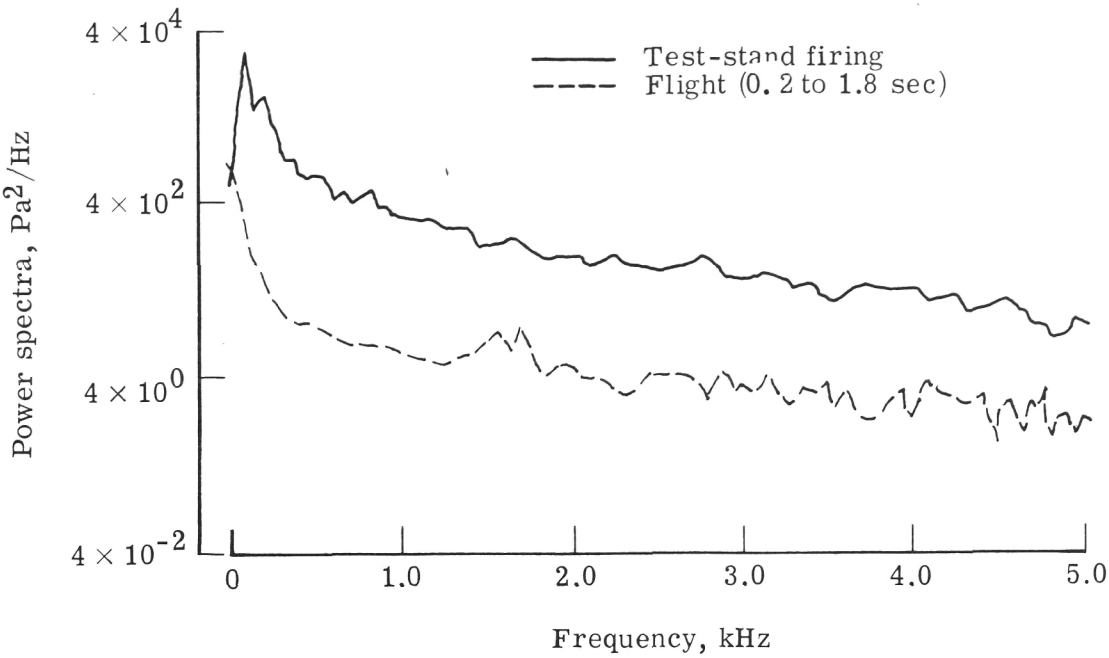

(f) Fluctuating pressure sensor, adapter section.

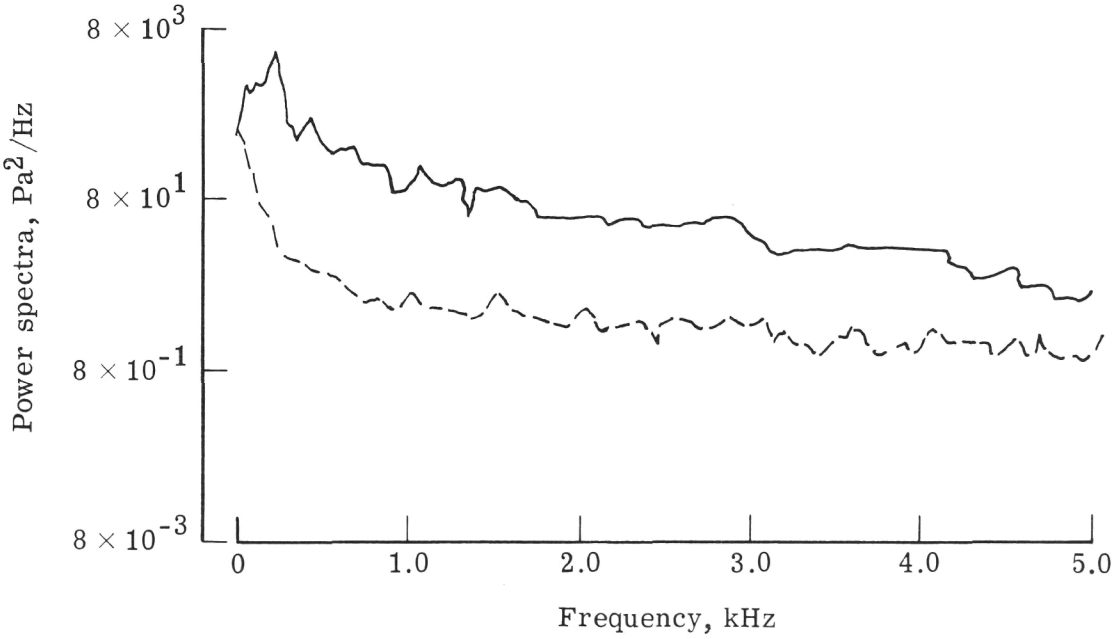

(g) Fluctuating pressure sensor, recovery system.

Figure 13.- Continued.

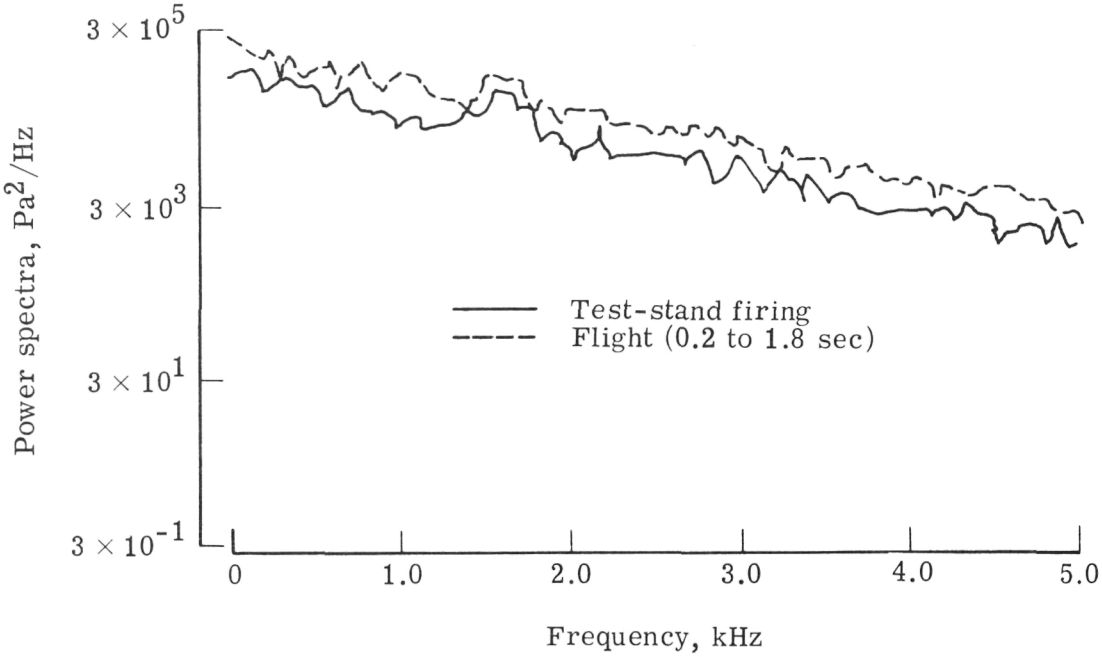

(h) Fluctuating pressure, nozzle.

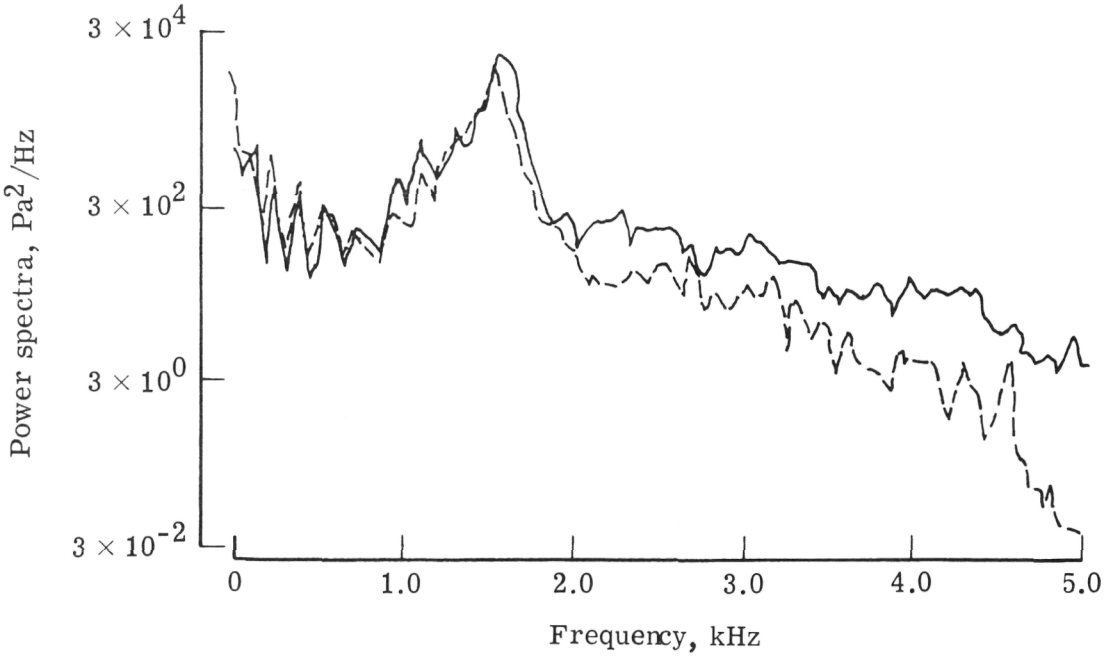

(i) Fluctuating pressure, headcap.

Figure 13.- Concluded.

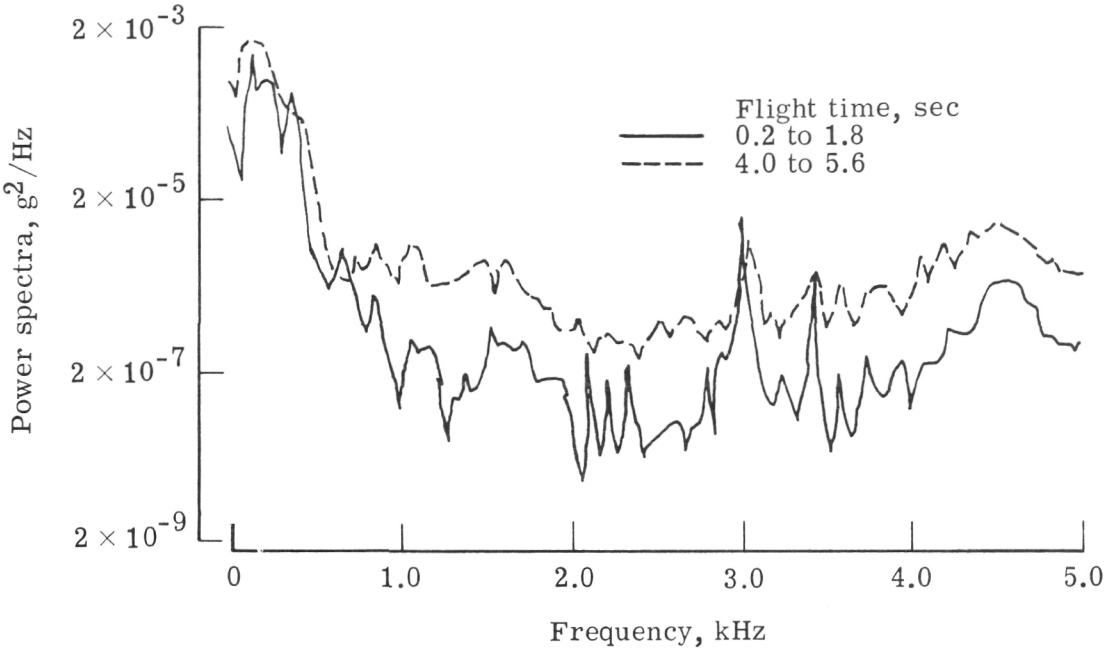

(a) Instrument post.

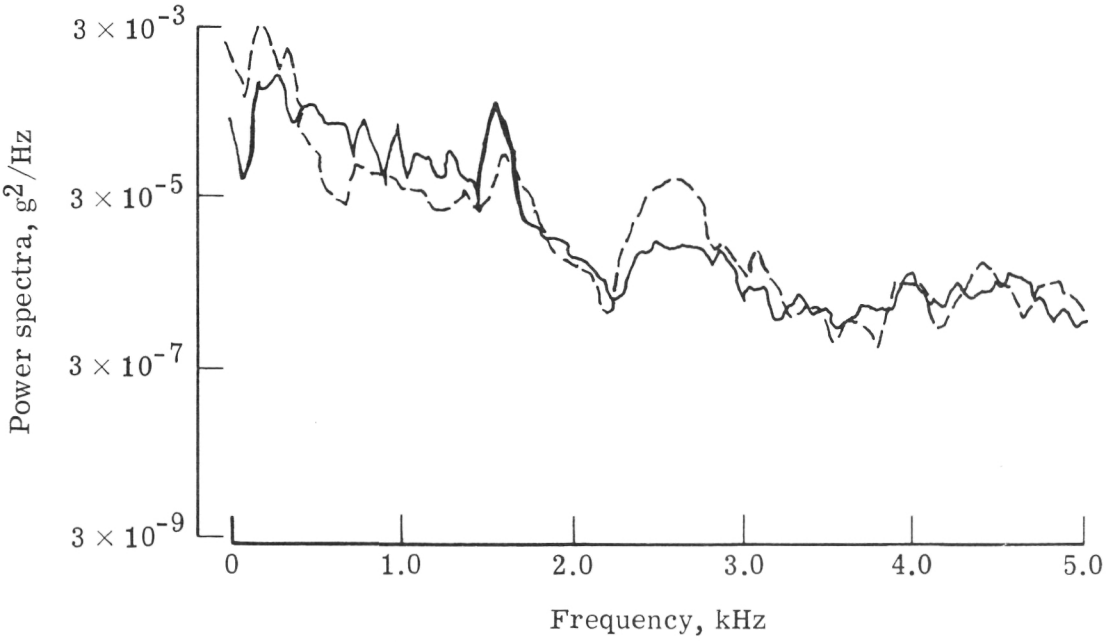

(b) Aft instrument post (lateral).

Figure 14.- Power spectral densities during flight. Burn times, 0.2 to 1.8 sec and 4.0 to 5.6 sec; 40-Hz bandwidth.

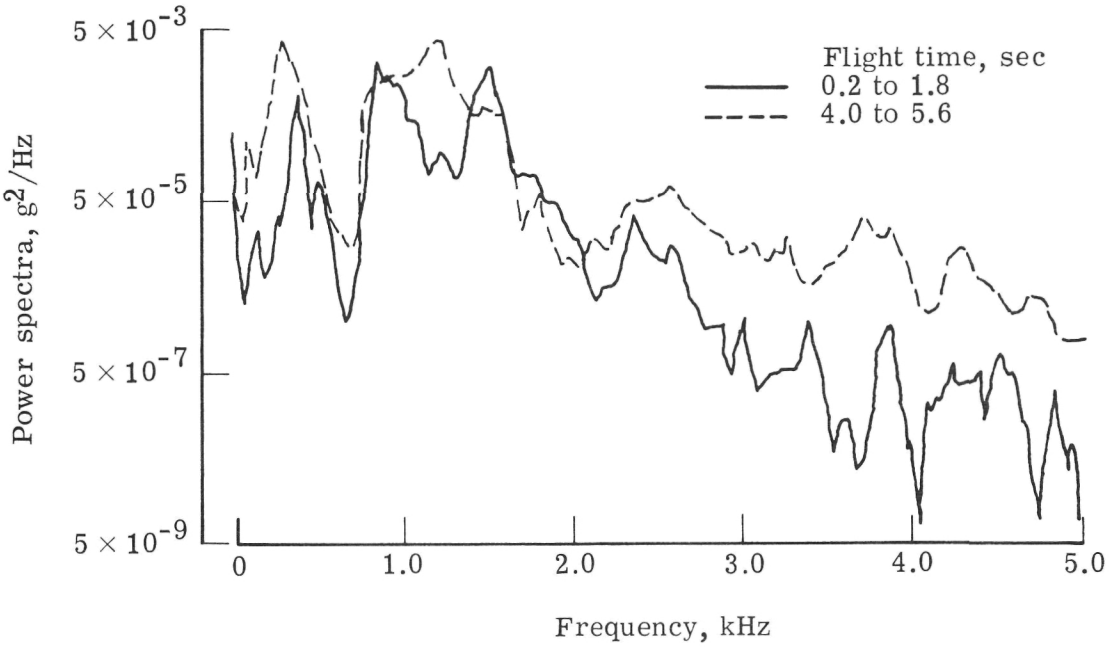

(c) Aft instrument post.

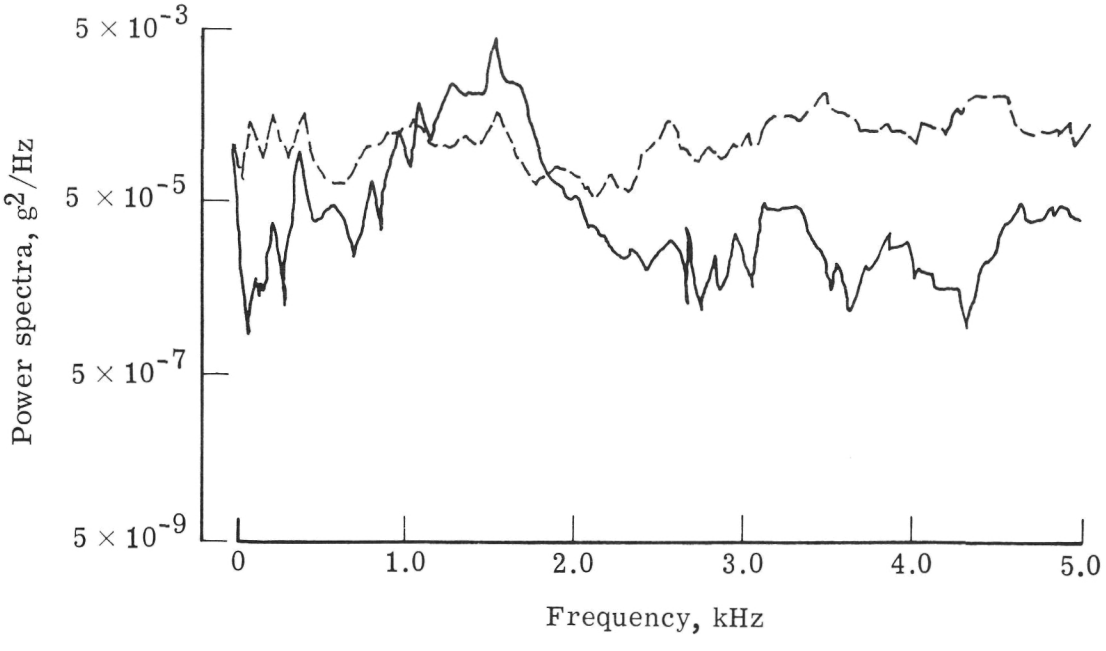

(d) Forward motor ring.

Figure 14.- Continued.

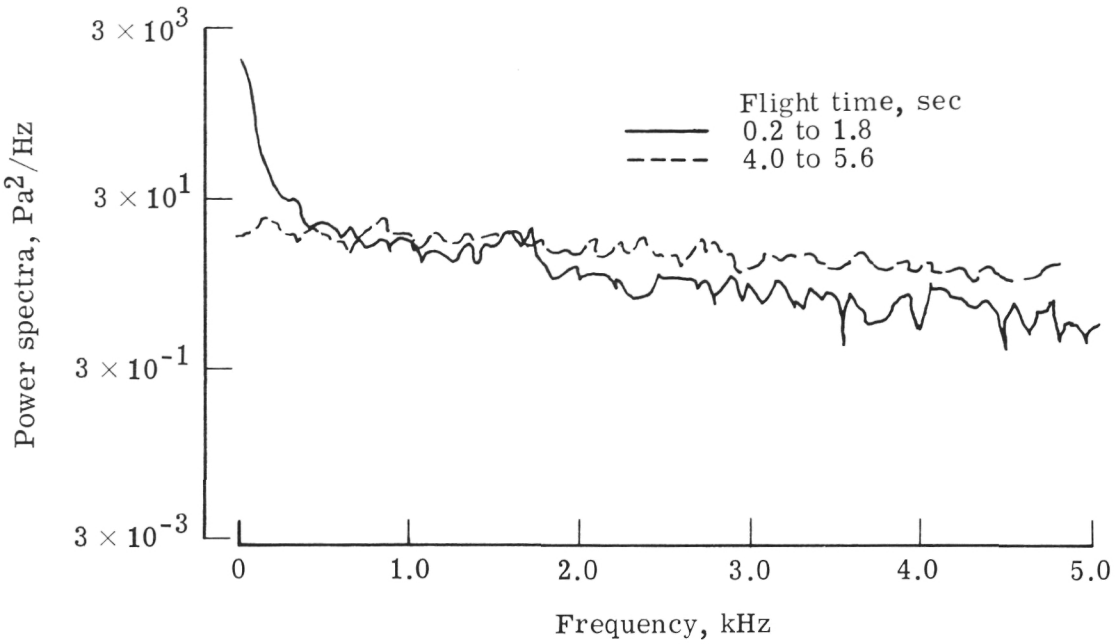

(e) Fluctuating pressure sensor, adapter section.

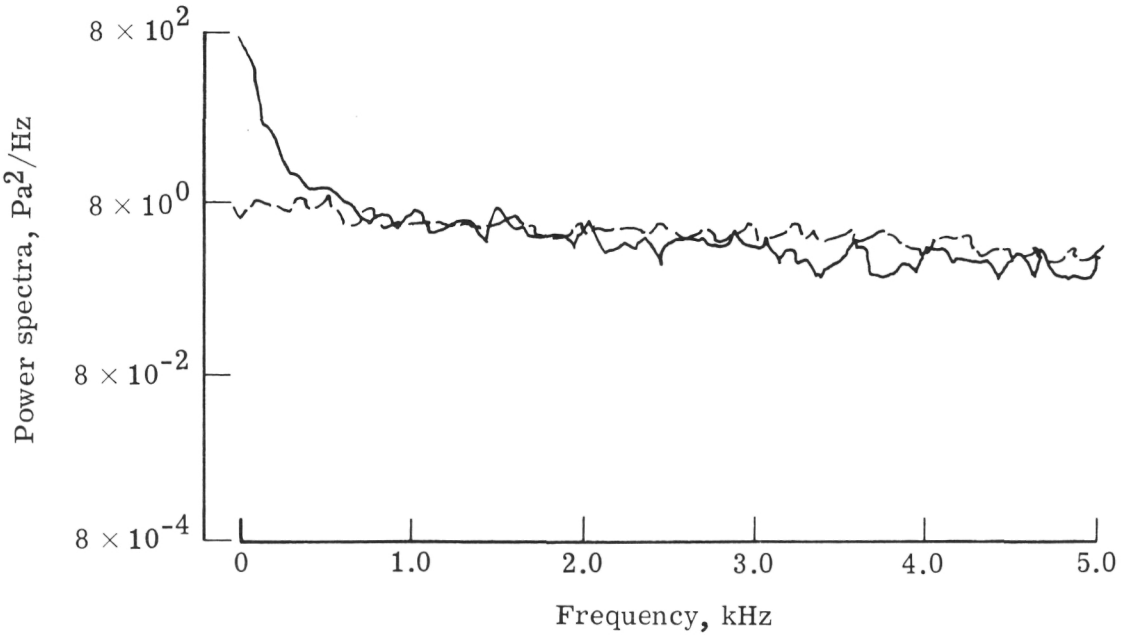

(f) Fluctuating pressure sensor, recovery section.

Figure 14.- Concluded.

NATIONAL AERONAUTICS AND SPACE ADMINISTRATION
WASHINGTON, D.C. 20546

OFFICIAL BUSINESS
PENALTY FOR PRIVATE USE $300

SPECIAL FOURTH-CLASS RATE
BOOK

POSTAGE AND FEES PAID
NATIONAL AERONAUTICS AND
SPACE ADMINISTRATION
451

U.S.MAIL

POSTMASTER : If Undeliverable (Section 158 Postal Manual) Do Not Return

"The aeronautical and space activities of the United States shall be conducted so as to contribute . . . to the expansion of human knowledge of phenomena in the atmosphere and space. The Administration shall provide for the widest practicable and appropriate dissemination of information concerning its activities and the results thereof."

—NATIONAL AERONAUTICS AND SPACE ACT OF 1958

NASA SCIENTIFIC AND TECHNICAL PUBLICATIONS

TECHNICAL REPORTS: Scientific and technical information considered important, complete, and a lasting contribution to existing knowledge.

TECHNICAL NOTES: Information less broad in scope but nevertheless of importance as a contribution to existing knowledge.

TECHNICAL MEMORANDUMS: Information receiving limited distribution because of preliminary data, security classification, or other reasons. Also includes conference proceedings with either limited or unlimited distribution.

CONTRACTOR REPORTS: Scientific and technical information generated under a NASA contract or grant and considered an important contribution to existing knowledge.

TECHNICAL TRANSLATIONS: Information published in a foreign language considered to merit NASA distribution in English.

SPECIAL PUBLICATIONS: Information derived from or of value to NASA activities. Publications include final reports of major projects, monographs, data compilations, handbooks, sourcebooks, and special bibliographies.

TECHNOLOGY UTILIZATION PUBLICATIONS: Information on technology used by NASA that may be of particular interest in commercial and other non-aerospace applications. Publications include Tech Briefs, Technology Utilization Reports and Technology Surveys.

Details on the availability of these publications may be obtained from:

SCIENTIFIC AND TECHNICAL INFORMATION OFFICE

NATIONAL AERONAUTICS AND SPACE ADMINISTRATION

Washington, D.C. 20546